

Modeling of the Alcohol Dehydrogenase Active Site: Two Different Modes of Alcohol Binding in Crystals of Zinc and Cadmium Tri-*tert*-butoxysilanethiolates Evidenced by X-ray Diffraction and Solid-State Vibrational Spectroscopy

Anna Dołęga,^{*[a]} Katarzyna Baranowska,^[a] Dietrich Gudat,^[b] Aleksander Herman,^[a] Janusz Stangret,^[c] Antoni Konitz,^[a] Maciej Śmiechowski,^[c] and Sylwia Godlewska^[a]

Dedicated to Professor Wiesław Wojnowski on the occasion of his 75th birthday

Keywords: Zinc / Cadmium / N,S ligands / Structure elucidation / Enzyme models / Coordination modes

Two different modes of binding methanol and ethanol were found in crystals of heteroleptic zinc and cadmium complexes with MS₂NO₂ and MS₂NO kernels and with a general formula M(RS)₂(im) (M = Zn, Cd; RS = tri-*tert*-butoxysilanethiolate; im = imidazole, 2-methylimidazole, 2-ethylimidazole). Alcohol molecules are either trapped in the crystal lattice by NH...O and OH...S hydrogen bonds or directly coordinated to the metal centre. The complexes were studied by X-ray diffraction, solid state FTIR and ¹H, ¹³C, ²⁹Si, and

¹¹³Cd NMR spectroscopy both in solution and the solid state. The zinc complexes containing coordinated methanol and ethanol are considered as structural mimics of the active site of alcohol dehydrogenase and support intermittent five-coordination of the zinc ion in the active site of alcohol dehydrogenase.

(© Wiley-VCH Verlag GmbH & Co. KGaA, 69451 Weinheim, Germany, 2009)

Introduction

Medium-chain, NAD⁺-dependent alcohol dehydrogenase (Zn-dependent ADH, EC 1.1.1.1) is a zinc enzyme, which catalyses the reversible oxidation of primary and secondary alcohols to aldehydes by utilising NAD⁺ as a co-substrate. The individual steps in the mechanism of action of the enzyme include: (i) NAD⁺ binding; (ii) Alcohol (substrate) binding to the catalytic zinc ion with concomitant displacement of a water molecule; (iii) Closing of the catalytic site (domain rotation). Residual water is expelled from the catalytic site, and the pK_a of the bound alcohol decreases. The alcohol dissociates and a proton is transported through the hydrogen-bond network out of the catalytic site; (iv) Hydride transfer from the zinc-bound alcoholate to the nicotinamide ring; (v) The leaving of the aldehyde group and replacement by a neutral water molecule; (vi) The opening of the catalytic

site and release of NADH.^[1] The mechanism may be summarised by the following Equation (1).



The horse liver form of the enzyme (liver alcohol dehydrogenase, LADH) is the most-extensively examined specimen among mammalian ADHs. The enzyme possesses one zinc ion in the active site and a second zinc ion in a noncatalytic site. The zinc ion in the active site is positioned at the bottom of the domain-separating cleft. It is bound by three protein ligands (Cys-46, His-67, and Cys-174) in a distorted tetrahedral coordination sphere, and the fourth coordination position is accessible to water or substrates.^[1b,1d]

There are a few points with regard to the detailed mechanism of action of ADH that are still under discussion. One of them is the coordination number of the Zn²⁺ ion located in the active site. The coordination of zinc in ADH is generally described as pseudotetrahedral,^[1] but there are several findings supporting pentacoordination of zinc during the catalytic cycle.^[2] A mechanism has been suggested in which a bound water molecule is not displaced from zinc, and the coordination sphere of the metal ion is thus expanded.^[2d] Furthermore, the perseverance of the water ligand is said to be crucial for the functioning of the enzyme, and its complete exclusion from the active site has been suggested to be a part of the inhibition process.^[2e]

[a] Department of Inorganic Chemistry, Gdańsk University of Technology, Narutowicza St. 11/12, 80-233, Gdańsk, Poland
Fax: +48-58 347 26 94
E-mail: ania@chem.pg.gda.pl

[b] Institut für Anorganische Chemie, Universität Stuttgart, Pfaffenwaldring 55, 70569 Stuttgart, Germany

[c] Department of Physical Chemistry, Gdańsk University of Technology, Narutowicza St. 11/12, 80-233, Gdańsk, Poland

Supporting information for this article is available on the WWW under <http://dx.doi.org/10.1002/ejic.200900106>.

The major source of information on the ADH structure and function comes from crystallographic data. The protein data bank lists 81 structures of EC 1.1.1.1 (alcohol dehydrogenase) gathered since 1984.^[3] Those obtained earlier were reviewed.^[1b] Alcohol dehydrogenase was also studied by various spectroscopic methods in the Co-, Mn-, Ni-, Cu-, ¹⁰⁹Cd-, and ¹¹³Cd-substituted forms.^[4] The available data on the activities and structures of the metal-substituted proteins indicate that information obtained in this way should be especially useful in the case of cobalt(II)- and, to a lesser extent, cadmium(II) substitution. Quite recently, a new method of investigation of the protonation status of metal-bound ligands was developed by Ryde et al.,^[5] who introduced DFT calculations into the crystal structure refinement and could thus obtain an improved *R* factor for the protein structure. Tests of this quantum refinement method have been performed on ADH.^[5b]

Studies on synthetic analogues, i.e. small molecules that resemble the structural and functional sites, of the enzymes are yet another way of elucidating the substrate–metal interaction.^[6] The existence of relatively simple syntheses of tri-*tert*-butoxysilanethiolates with MS₂NO₂ (M = Zn, Cd, Co, Mn) cores encouraged us to model the enzymatic centre of alcohol dehydrogenase.^[7] In our previous studies, we proved that heteroleptic cadmium tri-*tert*-butoxysilanethiolates with CdS₂NO₂ kernels exhibit very similar ¹¹³Cd NMR chemical shifts to that of LADH-NAD⁺.^[7k] Furthermore, it has recently been shown that methanol binds to manganese in an environment resembling the LADH catalytic centre.^[7j] The use of bulky thiolate ligands helps in these cases to overcome basic problems concerning the mimicking of enzymes with small molecule systems. These problems arise because of the differences between the coordination environments of zinc in enzymes and in small complexes^[6] and the tendency of metal thiolates to form S-bridged clusters.^[6,8]

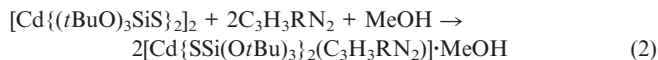
In this paper we demonstrate the ability of zinc and cadmium tri-*tert*-butoxysilanethiolates to bind methanol and ethanol in a coordination environment that mimics the active centre of alcohol dehydrogenase. The structural features of the zinc and cadmium complexes are described, and the solid-state FTIR spectra of the complexes in the OH and NH stretching regions are discussed. The stabilities of the cadmium complexes in methanol are evaluated on the basis of solution ¹³C and ¹¹³Cd NMR spectroscopy and HF calculations and are compared to the stabilities of analogous zinc complexes. ¹³C, ²⁹Si and ¹¹³Cd CP/MAS NMR spectra of the cadmium complexes are discussed and compared with ¹¹³Cd NMR spectra of cadmium-substituted alcohol dehydrogenase. Calculated energies for the deprotonation of free and zinc-bound ethanol are also compared.

Results and Discussion

Syntheses

The reactions of zinc and cadmium tri-*tert*-butoxysilanethiolates with imidazole, 2-methylimidazole and 2-ethyl-

imidazole led to the products **1–6c** described in Figure 1. The cadmium and zinc complexes were obtained by reactions (2) and (3) (R = H, Me, Et; R' = Me, Et, *i*Pr).



Almost all of the complexes crystallise at low temperature from the alcohol reaction mixtures after the addition of acetonitrile, in which they are poorly soluble. The exception is **4**, which does not contain a solvating alcohol molecule, and it was recrystallised from hexane. For a discussion on the features of the S ligand see the literature.^[7] In our previous work, we demonstrated the equilibrium character of the reaction of cadmium tri-*tert*-butoxysilanethiolate with 3,5-dimethylpyridine and 1-methylimidazole^[7k,9] in [D₈]toluene and CDCl₃. As we will show later in this paper, we have been able to prove the presence of similar equilibria for the reactions of cadmium tri-*tert*-butoxysilanethiolate with imidazole and 2-methylimidazole in methanol.

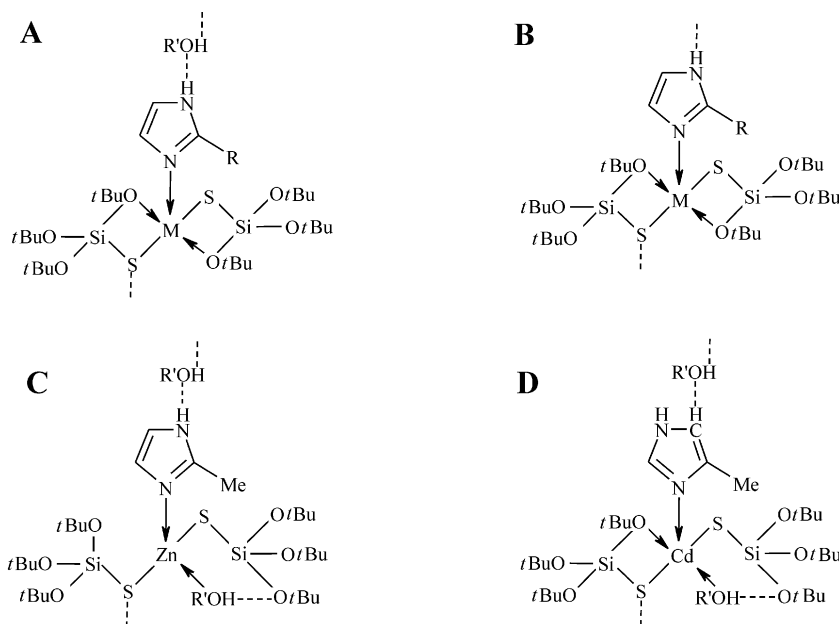
On removing the crystals from the supernatant solvent, most of the complexes lose the solvating alcohol molecule. In the case of **1**, this process is very fast, and after an hour, translucent crystals of **1** turn into a white powder.

Crystal Structures

Typical structural features of the obtained complexes as well as the most-common coordination geometries among them are exemplified by the molecular structure of **6b**, shown in Figure 2. The asymmetric unit of the crystals of **6b** contains two molecules of zinc thiolate and two molecules of alcohol. The metal ions are coordinated by two S (S1, S2 or S3, S4), one N (N1 or N3) and two O (O1, O4 or O7, O10) donor atoms, and the coordination geometry may be approximated as a strongly distorted trigonal bipyramid in which the Zn, N, S, S atoms define the basal trigonal plane and the oxygen atoms occupy apical positions (Figure 2). The S–Zn–S angle is the widest and one of the O–Zn–N angles is close to 90° as is usual. The Zn–O vectors intersect the basal plane in an oblique manner.^[7g,7h]

The solvating alcohol molecules link adjacent complexes through two NH⋯O and OH⋯S hydrogen bonds to give infinite, antiparallel chains. Molecular arrangements similar to that of **6b** are denoted as type **A** crystals in Figure 1. All type **A** systems are distinguished by: (i) the coordination pattern – the metal ion is surrounded by one imidazole molecule and two O,S-chelating tri-*tert*-butoxysilanethiolates, and (ii) the presence of solvating alcohol molecules that are inserted in a regular manner between the molecules of complex.

The important bond lengths and angles for **3**, **5d** and **6b**, which exhibit the same structural features, are listed in Table 1. Hydrogen-bond parameters for all complexes are gathered in Table 2.



No.	Formula	Compound	Structure Type	R	R'	Remarks
1.	$\{\text{Cd}[(t\text{BuO})_3\text{SiS}]_2(\text{C}_4\text{H}_6\text{N}_2)\} \cdot \text{CH}_3\text{OH}$	1	A	H	methyl	One molecule of complex in the independent unit
2.	$\{\text{Cd}[(t\text{BuO})_3\text{SiS}]_2(\text{C}_4\text{H}_6\text{N}_2)\} \cdot \text{CH}_3\text{OH}$ $\{\text{Cd}[(t\text{BuO})_3\text{SiS}]_2(\text{C}_4\text{H}_6\text{N}_2)(\text{CH}_3\text{OH})\}$	2a	A+D	methyl	methyl	Both cadmium ions pentacoordinated
3.	$\{\text{Cd}[(t\text{BuO})_3\text{SiS}]_2(\text{C}_4\text{H}_6\text{N}_2)\} \cdot \text{C}_2\text{H}_5\text{OH}$	2b	A?	methyl	ethyl	X-ray structure not determined
4.	$\{\text{Cd}[(t\text{BuO})_3\text{SiS}]_2(\text{C}_4\text{H}_6\text{N}_2)\} \cdot \text{CH}_3\text{OH}$	3	A	ethyl	methyl	Two molecules of complex in the independent unit
5.	$\{\text{Zn}[(t\text{BuO})_3\text{SiS}]_2(\text{C}_4\text{H}_6\text{N}_2)\}$	4	B	H	methyl	One molecule of complex in the independent unit. No solvate.
6.	$\{\text{Zn}[(t\text{BuO})_3\text{SiS}]_2(\text{C}_4\text{H}_6\text{N}_2)\} \cdot \text{CH}_3\text{OH}$ $\{\text{Zn}[(t\text{BuO})_3\text{SiS}]_2(\text{C}_4\text{H}_6\text{N}_2)(\text{CH}_3\text{OH})\}$	5a	A+C	methyl	methyl	One zinc ion pentacoordinated, one zinc ion tetraordinated
7.	$\{\text{Zn}[(t\text{BuO})_3\text{SiS}]_2(\text{C}_4\text{H}_6\text{N}_2)\} \cdot \text{C}_2\text{H}_5\text{OH}$	5b	A	methyl	ethyl	One molecule of complex in the independent unit
8.	$\{\text{Zn}[(t\text{BuO})_3\text{SiS}]_2(\text{C}_4\text{H}_6\text{N}_2)\}$ $\{\text{Zn}[(t\text{BuO})_3\text{SiS}]_2(\text{C}_4\text{H}_6\text{N}_2)(\text{C}_2\text{H}_5\text{OH})\}$	5c	B+C	methyl	ethyl	No solvating EtOH. Voids in the crystal
9.	$\{\text{Zn}[(t\text{BuO})_3\text{SiS}]_2(\text{C}_4\text{H}_6\text{N}_2)\} \cdot \text{C}_2\text{H}_5\text{OH}$	5d	A	methyl	2-propyl	Two molecules of complex in the independent unit
10.	$\{\text{Zn}[(t\text{BuO})_3\text{SiS}]_2(\text{C}_4\text{H}_6\text{N}_2)\} \cdot \text{CH}_3\text{OH}$	6a	A	ethyl	methyl	One molecule of complex in the independent unit
11.	$\{\text{Zn}[(t\text{BuO})_3\text{SiS}]_2(\text{C}_4\text{H}_6\text{N}_2)\} \cdot \text{C}_2\text{H}_5\text{OH}$	6b	A	ethyl	ethyl	Two molecules of complex in the independent unit
12.	$\{\text{Zn}[(t\text{BuO})_3\text{SiS}]_2(\text{C}_4\text{H}_6\text{N}_2)\} \cdot \text{C}_2\text{H}_5\text{OH}$	6c	A	ethyl	2-propyl	One molecule of complex in the independent unit [7]

Figure 1. Formulas and symbols of the compounds.

The molecular structures and crystal-packing motifs of **5b** and **6a** are also of type **A** and are merely distinguished from **3**, **5d** and **6b** by the presence of only one rather than two molecules of complexes and alcohol in the asymmetric unit. The molecular structure and the crystal-packing scheme of **5b** is shown in the Supporting Information as Figures S1 and S2, and important bond lengths and angles for **5b** and **6a** are given in Table S1.

Complex **1** crystallises in a different space group ($Pna2_1$), but nevertheless its molecular structure resembles those of

type **A** complexes. The molecular structure and the crystal-packing scheme are shown in Figure S3. The analogous zinc complex **4** does not contain a solvating alcohol molecule (Figure S4) and is thus assigned to structure type **B**. The imidazole ligand in **4** forms a $\text{NH}\cdots\text{S}$ hydrogen bond with the thiolate residue from a neighbouring molecule of the complex (Figure S4). Important bond lengths and angles for **1** and **4** are given in Table S2.

Somewhat surprisingly, with the use of 2-methylimidazole, cocrystals of two different coordination compounds

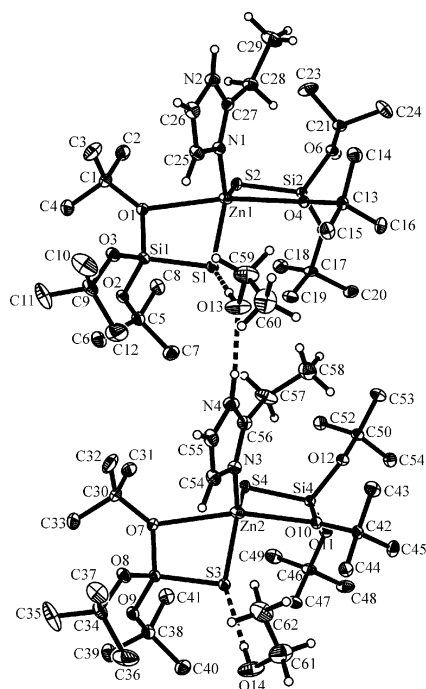


Figure 2. Molecular structure of **6b** with the labeling scheme (hydrogen atoms of *t*BuO groups are omitted). Displacement ellipsoids are drawn at the 30% probability level. Hydrogen bonds are indicated with dashed lines.

were obtained both for zinc and cadmium ions. In crystals of **2a** and **5a**, the alcohol molecules are either trapped in crystal voids and interact with metal silanethiolates through hydrogen bonds (e.g. O14–H14...S3 in **2a**, Figure 3, Table 3), or directly coordinated to the cadmium or zinc ions (e.g. Zn1–O13 in **5a**, Figure 4, Table 3). Interestingly, in the complexes with the coordinated methanol, there is a difference between the zinc and cadmium coordination numbers, which did not manifest in the type **A** complexes. The coordination number of cadmium is five for both complexes in crystals **2a**, since methanol replaces one of the chelating *tert*-butoxy groups and the other *tert*-butoxy group is still bonded to Cd1 (Figure 3). In **5a**, complexation of methanol causes a lowering of the coordination number of zinc from five to four (Figure 4). However, it must be noted that the Zn1–O1 distance

(2.984 Å) is still significantly shorter than Zn1–O2 (4.442 Å) and Zn1–O3 (4.653 Å), which may suggest a very weak bonding interaction. The angle S1–Zn1–S2 (120.35°) in **5a** is at the border between those of penta- and tetraordinated zinc tri-*tert*-butoxysilanethiolates.^[7n] The M–O bond is significantly shorter for methanol binding than for *t*BuO binding in both the zinc and cadmium complexes (Table 3).

The crystal packing is not exactly the same in **2a** and **5a**. In the crystals of **5a**, a solvating methanol molecule is inserted between two molecules of the complex and forms two NH...O and OH...S hydrogen bonds similar to those of solvating alcohol molecules in complexes **1**, **3**, **5b**, **5d**, **6a** and **6b**. There is also an NH...S hydrogen-bond interaction between the adjacent molecules of the complex (Figure 5a). The solvating methanol present in the crystals of **2a** forms only one hydrogen bond, OH...S, as if it were half way “pushed out” of the chain. All molecules of cadmium thiolate in a chain interact directly through NH...S hydrogen bonds (Figure 5b). Another very weak interaction in the crystals of **2a** is C26H26...O14. If it is incorporated into the picture, a ladderlike net of weak hydrogen bonds may be considered in the crystals of **2a** (Figure 5c). It can be seen that despite the similar stoichiometries and structures of **2a** and **5a**, the methanol molecule in each case is trapped in a slightly different position and with a different hydrogen-bonding pattern. The binding of methanol in previously described manganese tri-*tert*-butoxysilanethiolate^[7j] resembles that in **2a**. Because of these small differences we decided to denote crystals of **2a** as type **D** and crystals of **5a** as type **C**.

By changing the temperature of crystallisation and the concentration of ethanol in the solution, we were also able to obtain crystals of the zinc complexes with ethanol complexed to zinc (**5c**, Figure 6) or merely as a solvating group (**5b**, Figures S1 and S2). Thus, the binding of alcohol to the metal centre is an easily reversible process. Diffraction data obtained for **5c** indicate, in concordance with the elemental analysis, that crystals of **5c** do not contain solvating alcohol; therefore, the structure can be described as a mixture of types **B** and **C**.

The zinc coordination environment during the second step of catalysis (alcohol binding) in the LADH active site

Table 1. Selected bond lengths [Å] and angles [°] for **3**, **5d** and **6b**.

	3 ^[a]	5d	6b		3 ^[a]	5d	6b
Zn1–N1	2.227(3)	2.0103(16)	2.0030(17)	S1–Zn1–S2	133.56(3)	130.170(19)	127.47(2)
Zn1–S1	2.4691(8)	2.2815(5)	2.2872(5)	O1–Zn1–O4	162.80(6)	164.29(4)	168.68(5)
Zn1–S2	2.4478(8)	2.2719(5)	2.2762(5)	N1–Zn1–O1	93.79(8)	94.29(5)	90.83(6)
Zn1–O1	2.5856(19)	2.5632(13)	2.5545(14)	N1–Zn1–O4	103.10(8)	101.14(5)	100.27(6)
Zn1–O4	2.5694(19)	2.3914(12)	2.3879(13)	S1–Zn1–O1	71.19(5)	73.53(3)	74.10(3)
Zn2–N3	2.237(3)	2.0113(16)	2.0199(17)	S2–Zn1–O1	102.20(5)	97.61(3)	98.37(3)
Zn2–S3	2.4650(8)	2.2891(5)	2.2879(5)	N3–Zn2–S3	106.60(7)	110.99(5)	109.44(5)
Zn2–S4	2.4364(8)	2.2845(5)	2.2647(5)	N3–Zn2–S4	116.88(8)	120.40(5)	118.95(5)
Zn2–O7	2.610(2)	2.5320(13)	2.5754(14)	S3–Zn2–S4	136.44(3)	128.459(19)	131.18(2)
Zn2–O10	2.6030(19)	2.3856(12)	2.4511 (13)	O7–Zn2–O10	158.02(7)	167.02(4)	159.16(5)
N1–Zn1–S1	107.26(7)	110.86(5)	111.09(5)	N3–Zn2–O7	95.22(8)	92.60(5)	94.86(6)
N1–Zn1–S2	119.12(7)	118.74(5)	121.08(5)	N3–Zn2–O10	106.45(8)	99.97(5)	105.86(6)

[a] Cd1 instead of Zn1.

Table 2. Hydrogen-bond parameters.

Compound	Bond	D–H [Å]	H⋯A [Å]	D⋯A [Å]	∠DHA [°]
1	N2–H2A⋯O7 ⁱ	0.88	2.07	2.766(7)	135.7
	O7–H7⋯S2	0.84	2.37	3.210(4)	173
2a	N2–H2⋯S4 ⁱ	0.88	2.48	3.324(4)	160.2
	N4–H4⋯S1 ⁱⁱ	0.88	2.61	3.453(4)	161.9
	O13–H13A⋯O4	0.84	1.91	2.686(4)	152.3
	O14–H14D⋯S3	0.84	2.31	3.135(9)	166
3	N2–H2⋯O14 ⁱ	0.88	1.91	2.782(4)	168.8
	N4–H4⋯O13	0.88	1.9	2.777(4)	176
	O13–H13D⋯S1 ⁱⁱⁱ	0.84	2.39	3.174(3)	154.7
	O14–H14D⋯S3 ⁱⁱ	0.84	2.34	3.164(3)	165.5
5a	N2–H2⋯O14	0.88	1.88	2.755(4)	170.4
	N4–H4⋯S1 ⁱ	0.88	2.55	3.396(3)	160.9
	O13–H13D⋯O4	0.84	1.9	2.676(3)	152.7
	O14–H14D⋯S3 ⁱⁱ	0.84	2.32	3.105(3)	156.4
5b	N2–H2⋯O7 ⁱ	0.88	1.89	2.762(2)	174.5
	O7–H7⋯S2 ⁱⁱ	0.84	2.36	3.1840(17)	168.5
5c	N2–H2⋯S4 ⁱ	0.88	2.38	3.130(9)	143.2
	N4–H4⋯S1	0.88	2.45	3.286(4)	159.4
	O13–H13A⋯O4	0.982(10)	1.703(17)	2.659(4)	164(4)
5d	N2–H2⋯O14 ⁱ	0.88	1.9	2.765(2)	168.1
	N4–H4⋯O13 ⁱⁱ	0.88	1.9	2.778(2)	171.7
	O13–H13⋯S1	0.84	2.36	3.1951(14)	175.1
	O14–H14⋯S3	0.84	2.4	3.2349(14)	172.5
6a	N2–H2⋯O7 ⁱ	0.88	1.94	2.819(4)	172.3
	O7–H7⋯S2 ⁱⁱ	0.84	2.38	3.199(3)	164.5
6b	N2–H2⋯O14 ⁱ	0.88	1.89	2.759(3)	169.2
	N4–H4⋯O13	0.88	1.94	2.813(3)	173.1
	O13–H13⋯S1 ⁱⁱ	0.84	2.34	3.1614(18)	166.9
	O14–H14⋯S3 ⁱⁱⁱ	0.84	2.4	3.2430(18)	179.1
6c ^[7]	N2–H2⋯O7 ⁱ	0.88	1.89	2.774(2)	178.5
	O7–H7⋯S2 ⁱⁱ	0.84	2.37	3.1976(16)	167.7

1 i (0.5 + x, 0.5 – y, z)

2a i (–1 + x, y, z); ii (0.5 + x, 0.5 – y, 0.5 + z)

3 i (1 + x, y, –1 + z); ii (1 – x, –0.5 + y, 1.5 – z); iii (1 – x, 0.5 + y, 0.5 – z)

5a i (–0.5 + x, 0.5 – y, –0.5 + z); ii (1 + x, y, z)

5b i (–2 + x, 3.5 – y, 1.5 + z); ii (–1 + x, 3.5 – y, 0.5 + z)

5c i (x, –1 + y, z)

5d i (–1 + x, 1.5 – y, –0.5 + z); ii (x, 1.5 – y, 0.5 + z)

6a i (1 + x, 1.5 – y, –0.5 + z); ii (x, 1.5 – y, 0.5 + z)

6b i (x, y, –1 + z); ii (1 + x, 1.5 – y, 0.5 – z); iii (x, 1.5 – y, 0.5 – z)

6c i (x, 1.5 – y, –0.5 + z); ii (1 + x, 1.5 – y, 0.5 + z)

is reproduced in **5c** (Figure 7a). Together **5a** and **5c** are the first neutral zinc complexes that model the substrate-bound LADH active site, and **2a** is their cadmium analogue. Previously described model complexes, capable of alcohol binding, are either ionic^[10] or structurally different from ADH.^[11]

The zinc ion in the active site of liver alcohol dehydrogenase (LADH) is positioned at the bottom of the domain-separating cleft about 20 Å from the protein surface. It is bound by three protein ligands (Cys-47, His-67 and Cys-174), and the fourth coordination position is accessible to water molecules and other ligands from the solution (Fig-

ure 7b). The side chain of His-67 is additionally positioned in such a way that a hydrogen bond from the imidazole N3 atom to the carboxyl group of Asp-49 forms.^[1b,1d] Glu-68, which is highly conserved and is necessary for enzyme activity,^[12] is placed in the second coordination sphere of zinc in horse liver alcohol dehydrogenase (HLADH), whereas the same or corresponding glutamate residues in *S. Solfataricus* ADH and sorbitol dehydrogenase from silverleaf whitefly^[1c] were found to be ligands to zinc (Figure 8a–c). Moreover, two different coordination environments of the zinc atoms in the active site are observed in human glutathione-dependent formaldehyde dehydrogenase FDH. In the

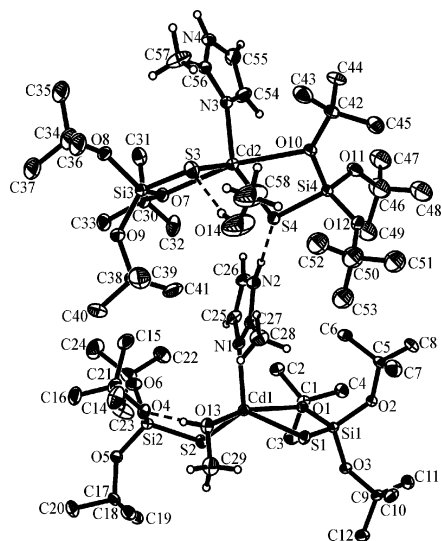


Figure 3. Molecular structure of **2a** with the labeling scheme (hydrogen atoms of *t*BuO groups are omitted). Thermal ellipsoids drawn at the 30% probability level.

FDH apoenzyme (here the term apoenzyme stands for an open conformation of FDH without the NAD⁺ cofactor, but with catalytic zinc), the zinc atom in the active site is coordinated to Cys-44, His-66, Cys-173 and a water molecule similar to that in HLADH. In the inhibited FDH·NAD(H), Glu-67 is coordinated to zinc instead of a water molecule, thus the zinc ions are capable of exchanging protein ligands (Figure 8d).^[13] It is probable that this “flexible Glu” (this term is taken from the literature^[1c]) can occupy alternative positions also in HLADH.^[1c] Ryde suggested^[12b] that the motion of the charged carboxylate group at Glu-68 inside the void may tune the actual partial charge on the zinc ion and speed up ligand exchange during the catalytic cycle. By means of quantum chemical and molecular mechanical geometry optimisations he showed that such a coordination can be accomplished with small changes in the geometry of the zinc coordination sphere and is kinetically favourable.^[12b] Oscillation of the apical O ligands at the zinc ion may also explain the spectroscopic

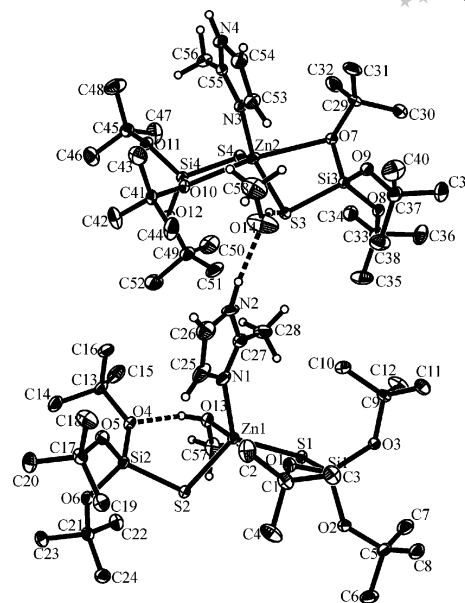


Figure 4. Molecular structure of **5a** with the labeling scheme (hydrogen atoms of *t*BuO groups are omitted). Thermal ellipsoids drawn at the 30% probability level.

properties of the Co- and Cd-substituted enzyme, which indicate the presence of five-coordinate metal centres in ADH.^[4d,4f,7j,7k] Figure 8 summarises variations in the zinc coordination spheres in different ADHs represented by HLADH,^[1b] sorbitol dehydrogenase,^[14] *Aeropyrum pernix* alcohol dehydrogenase complexed with octanoic acid^[15] and formaldehyde dehydrogenase.^[13]

In Table 4, we compare the structural data of **5a–d** to that of several structures of LADH ternary complexes deposited in the PDB protein data base (e.g. alcohol dehydrogenase bound with cofactor NADH and substrate).^[16] Nonmutant enzyme structures of the mammalian liver form of the enzyme have been chosen for comparison. The structural data of the active sites of various ADH proteins resemble that determined for heteroleptic, pentacoordinate zinc tri-*tert*-butoxysilanethiolates. The S–Zn–S angle in all pentacoordinate model zinc complexes with a ZnNO₂S₂

Table 3. Selected bond lengths [Å] and angles [°] for **2a**, **5a** and **5c**.

	2a ^[a]	5a	5c		2a ^[a]	5a	5c
Zn1–N1	2.233(4)	2.004(2)	2.002(13) (av.)	N1–Zn1–O1	95.81(12)	–	–
Zn1–S1	2.4788(11)	2.2851(7)	2.2826(11)	N1–Zn1–O13	93.96(13)	94.36(9)	92.8(3)
Zn1–S2	2.4572(11)	2.2792(8)	2.2818(12)	S1–Zn1–O1	69.05(6)	–	–
Zn1–O1	2.765(3)	–	2.5545(14)	S2–Zn1–O1	94.03(6)	–	–
Zn1–O13	2.416(3)	2.1359(19)	2.143(3)	S1–Zn1–O13	91.09(8)	101.53(6)	100.29(9)
Zn2–N3	2.242(4)	2.006(2)	1.998(3)	S2–Zn1–O13	96.88(8)	100.78(6)	101.32(9)
Zn2–S3	2.4632(13)	2.2831(8)	2.2632(11)	N3–Zn2–S3	115.49(11)	114.66(8)	120.59(10)
Zn2–S4	2.4664(12)	2.2709(8)	2.2908(12)	N3–Zn2–S4	114.74(11)	119.55(8)	110.57(10)
Zn2–O7	2.560(3)	2.5832(19)	2.512(3)	S3–Zn2–S4	129.64(4)	125.69(3)	128.80(4)
Zn2–O10	2.586(3)	2.4034(19)	2.460(3)	O7–Zn2–O10	167.40(9)	171.59(6)	168.95(9)
N1–Zn1–S1	112.00(10)	118.39(8)	116.3(3) (av.)	N3–Zn2–O7	97.76(12)	73.40(5)	96.86(12)
N1–Zn1–S2	117.54(10)	114.08(9)	115.3(3) (av.)	N3–Zn2–O10	92.25(12)	97.75(8)	93.56(12)
S1–Zn1–S2	128.98(4)	120.35(3)	121.64(4)	S3–Zn2–O7	72.21(7)	88.01(8)	75.62(7)
O1–Zn1–O13	159.98(10)	–	–	S4–Zn1–O7	97.69(7)	104.77(5)	97.55(7)

[a] Cd1 instead of Zn1.

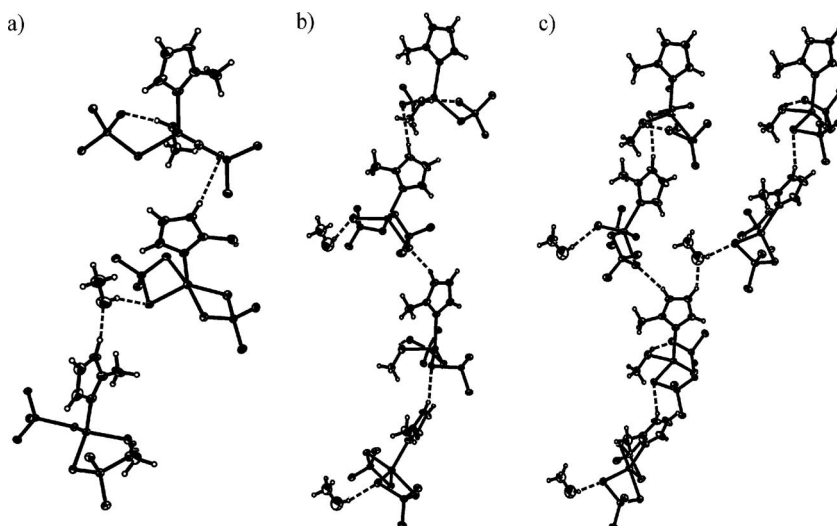


Figure 5. Crystal packing of (a) **5a**; (b) **2a** without CH...O interactions; (c) **2a** including CH...O interactions.

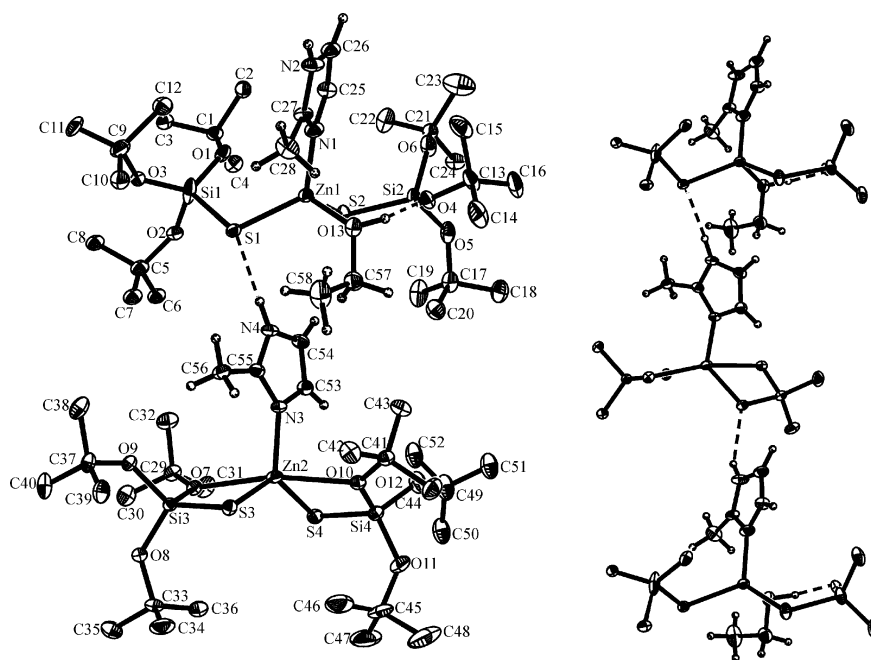


Figure 6. Molecular structure with the labeling scheme and crystal packing of **5c** (hydrogen atoms of *t*BuO groups are omitted, only one part of each disordered group is shown). Thermal ellipsoids drawn at the 30% probability level.

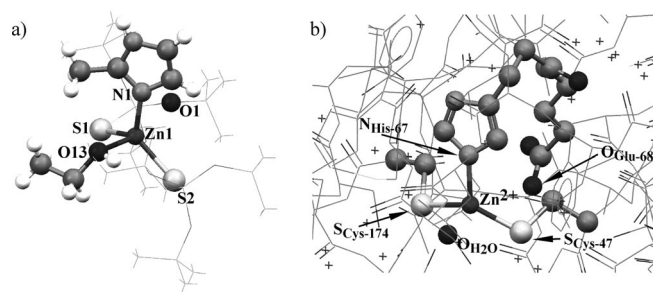


Figure 7. (a) Fragment of **5c** showing zinc coordination; (b) the active site of a horse liver dehydrogenase (Figure prepared from the PDB entry 1YE3^[167]).

kernel is very wide and ranges from 125.69(3) to 139.40(4), as found in this study and as reported in the literature;^[7a,7e–7g,7i] this angle decreases to 107.13(6)–120.35(3) in tetrahedral ZnNOS₂ and ZnN₂S₂ species.^[7e,7m,7n] The two populations of the S–Zn–S angles in the model ZnNOS₂ and ZnNO₂S₂ complexes are represented in Figure 9. When the coordination geometry of the zinc atom changes from a distorted trigonal-bipyramidal structure to a tetrahedral geometry, one of the oxygen atoms approaches the zinc atom and the second Zn–O distance increases, such that the difference between the Zn–O bonds lengths becomes larger. This change is accompanied by a decrease in the value of the S–Zn–S angle as shown in Figure 9. The O–Zn–N angle is always close to 90° in five-coordinate ZnNO₂S₂ com-

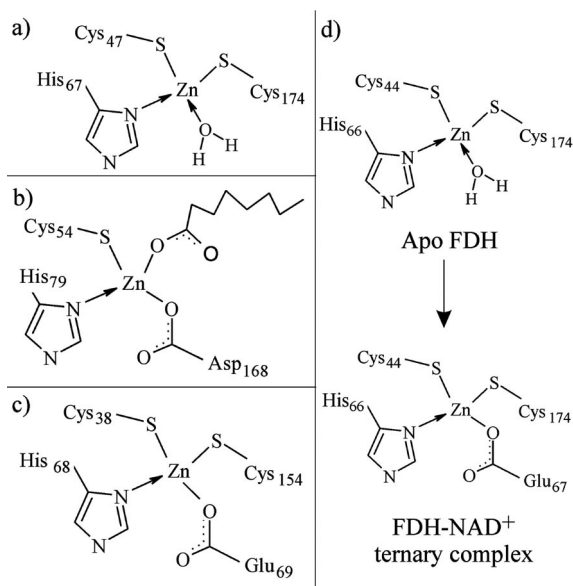


Figure 8. Coordination of catalytic zinc in various ADHs: (a) HLADH;^[1b] (b) *A. Pernix* ADH;^[15] (c) silverleaf whitefly SDH;^[14] (d) two forms of human FDH.^[13]

plexes. Since the S–Zn–S angles in the active site of ADH proteins are also very wide and the $O_{\text{substrate}}\text{--Zn--N}$ angle approaches 90° , we concluded that the zinc atom in the

active site is pentacoordinate with a coordination geometry that is similar to that presented in the model compounds. Thus, there should be a ligand opposite to the O-coordinated substrate in the active site of the ADHs, and the only likely candidate is the Glu-68 residue at a distance of 4.52–4.98 Å from Zn^{2+} in each structure. The Glu-68 side chain is placed in a void “behind” the active site – opposite to the substrate molecule (Figure 8). The $O_{\text{substrate}}\text{--Zn--}O_{\text{Glu-68}}$ angle in the compared ADHs, which is between 155.6 and 166.8° , is close to the O–Zn–O angle in the studied pentacoordinate zinc complexes [$164.29(4)$ –

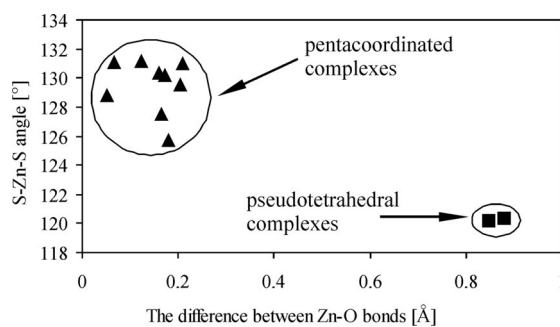


Figure 9. Two populations of S–Zn–S angle values in the complexes studied.

Table 4. Comparison of structural data for alcohol dehydrogenase^[16] and model zinc tri-*tert*-butoxysilanethiolates with 2-methylimidazole as coligand: **5a**, **5b**, **5c** and **5d**.

	ADH ^[16]						Model complexes				
	1HET	HLD	MG0	2OHX	1PIR	1YE3	5a ^[d]	5b ^[d]	5c ^[d]	5d ^[d]	
PDB symbol ^[16]	1HET	HLD	MG0	2OHX	1PIR	1YE3	5a ^[d]	5b ^[d]	5c ^[d]	5d ^[d]	
O ligand	OH [−]	[a]	[b]	DMSO	[c]	H ₂ O	Methanol / chelating <i>t</i> BuO	chelating <i>t</i> BuO	Ethanol / chelating <i>t</i> BuO	chelating <i>t</i> BuO	
Resolution [Å]	1.1	2.1	1.8	1.8	1.57	1.59	0.84	0.84	0.84	0.84	
Bond [Å]											
Zn–S	2.28	2.19	2.31	2.23	2.24	2.21	Zn1–S1	2.2792(8)	2.2773(5)	2.2826(11)	2.2815(5)
	2.26	2.23	2.27	2.19	2.23		Zn1–S2	2.2851(7)	2.2910(5)	2.2818(12)	2.2719(5)
Zn–S	2.29	2.20	2.31	2.32	2.27	2.42	Zn2–S3	2.2831(8)	–	2.2632(11)	2.2891(5)
	2.30	2.30	2.34	2.25	2.29		Zn2–S4	2.2709(8)	–	2.2908(12)	2.2845(5)
Zn–O	2.12	2.12/2.05	2.15	2.26	2.10	2.11	Zn1–O1	–	2.3722(13)	–	2.5632(13)
	2.11	2.19/2.04	2.18	2.13	2.15		Zn1–O4/Zn1–O13	2.1359(19)	2.5761(14)	2.143(3)	2.3914(12)
Zn–O _{Glu}	4.62	5.01	4.70	4.68	4.68	4.98	Zn2–O7	2.5832(19)	–	2.512(3)	2.5320(13)
	4.70	4.96	4.80	4.70	4.52		Zn2–O10	2.4034(19)	–	2.460(3)	2.3856(12)
Zn–N	2.09	2.21	2.10	2.14	2.04	2.05	Zn1–N1	2.004(2)	2.0093(17)	1.987(13)	2.0103(16)
	2.11	2.23	2.11	2.02	2.06		Zn2–N3	2.006(2)	–	1.998(3) ^[e]	2.0113(16)
Angle [°]											
S–Zn–S	133.0	121.5	122.1	130.2	128.2	129.3	S1–Zn1–S2	120.35(3)	129.50(2)	121.64(4)	130.170(19)
	132.8	129.3	125.0	129.4	129.2		S3–Zn2–S4	125.69(3)	–	128.80(4)	128.459(19)
O–Zn–N	85.6	88.7/94.3	91.0	93.8	91.4	101.3	O1–Zn1–N1	–	100.02(6)	–	94.29(5)
	83.6	83.3/90.8	91.8	94.2	90.9		O4/O13–Zn1–N1	94.36(9)	94.36(6)	89.6(3) ^[e]	101.14(5)
O–Zn–O _{Glu}	167.1	161.5/163.3	164.5	166.8	164.6	155.6	O7–Zn2–N3	88.01(8)	–	96.86(12)	92.60(5)
	164.6	153.6/159.8	163.1	166.8	164.5		O10–Zn2–N3	97.95(8)	–	93.56(12)	99.97(5)
							O1–Zn1–O4	–	165.26(5)	–	164.29(4)
							O7–Zn2–O10	171.59(6)	–	168.95(9)	167.02(4)

[a] Pentafluorobenzyl alcohol. [b] 2,3-difluorobenzyl alcohol. [c] N-1-methylhexylformamide. [d] This work. [e] Only one part of the disordered molecule is given.

171.59(6)°, Table 4]. These findings support the idea of Ryde that Glu-68 can be, at least intermittently, bonded to zinc.^[12b]

Vibrational Spectra

We analysed the positions of the NH and OH stretching bands in the FTIR spectra of **1–6c**, which was not easy as these bands strongly overlap and some of the crystals (especially **1**) quickly lose solvating alcohol. In order to locate the NH \cdots O and OH \cdots S stretching bands, FTIR ATR spectra of tri-*tert*-butoxysilanethiol/methanol (molar ratio 1:1) and 2-methylimidazole/methanol (molar ratio 0.25:1) mixtures were measured. The results – together with the suggested assignments of the IR bands – are shown in Figures 10 and 11. In the systems studied, the NH \cdots X stretching modes are found at $\approx 3200\text{ cm}^{-1}$ and are redshifted relative to the OH \cdots X bands, which are located in the range $3310\text{--}3480\text{ cm}^{-1}$.

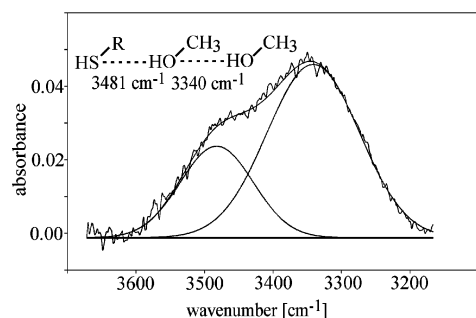


Figure 10. FTIR ATR spectrum of tri-*tert*-butoxysilanethiol/methanol mixture.

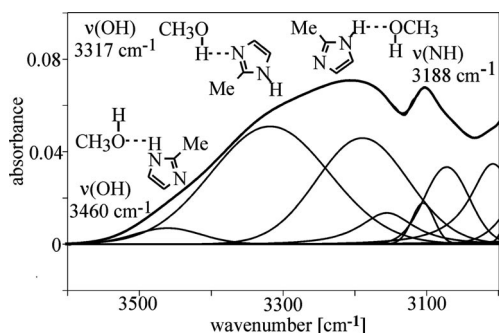


Figure 11. FTIR ATR spectrum of 2-methylimidazole/methanol mixture.

The relevant regions of the spectra obtained for the complexes are shown in Figures 12, 13 and 14. The full range ($4000\text{--}700\text{ cm}^{-1}$) FTIR solid state spectra of the studied compounds are available as Supporting Information (Figures S16–S27). The calculated analytical components of the spectra together with the suggested assignment are presented in Table 5. Deconvolutions of the spectra are available as Supporting Information (Figures S5–S15). The spectra of **5b**, **5d**, **6a**, **6b** and **6c** (Figure 12) have very similar shapes in the OH and NH stretching region. Broad but

well-resolved OH (OH \cdots S) and NH (NH \cdots O) stretching bands can easily be discerned. Their maxima are listed in Table 5. On the other hand, there are no well-defined OH stretching bands in the spectra of **1** and **4**, presented in Figure 13. This apparent contradiction to the crystal structure data of **1** can be resolved if we assume that the methanol that had been detected in the crystals of **1** by low-temperature X-ray diffraction experiments is very weakly bound and is almost entirely lost during the preparation for the FTIR measurements; the crystals are broken into very thin fragments.

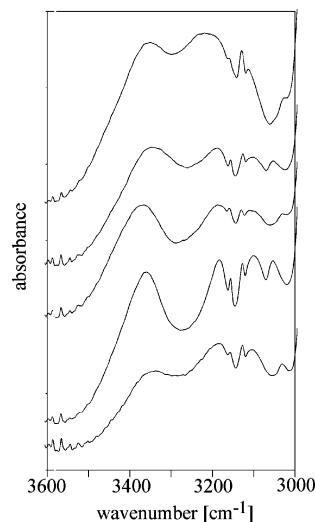


Figure 12. FTIR spectra of **6b**, **5d**, **6c**, **5b** and **6a** (from the bottom) in the OH and NH stretching region.

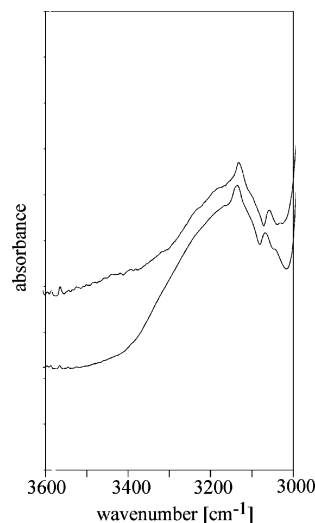


Figure 13. FTIR spectra of **1** (upper spectrum) and **4**.

The influence of the hydrogen-bond types and lengths on the location of the IR bands is best illustrated by comparison of the spectrum of **5b** with that of **5c** (Figure 14). Exchange of OH \cdots S by OH \cdots O results in a redshift of the OH stretching band, as could be expected from the relative strengths of these hydrogen bonds (Figure 14, Table 5). The same can be stated for the NH \cdots S and NH \cdots O interactions;

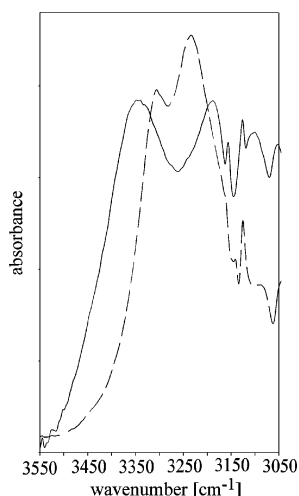


Figure 14. FTIR spectra of **5b** (solid line) and **5c** (dashed line) in the OH and NH stretching region.

the NH stretching bands are located at 3234 cm^{-1} for **5c** and at 3209 cm^{-1} for **5b**, and the shift is in concordance

Table 5. Analytical components of FTIR bands of **1–6c** in the OH and NH stretching region.

	Metal	Alcohol	Imidazole	Component in OH/NH stretching region [cm^{-1}]	Assignment
1	Cd	methanol	H	3400 (v. br., w) 3330 (v. br., w) 3214 (br., vs)	OH – undefined? OH – undefined? NH – undefined
2a	Cd	methanol	2-methyl	3311 cm^{-1} (v. br., m) 3236 cm^{-1} (br., s) 3171 cm^{-1} (br., s)	OH \cdots O NH \cdots S NH \cdots O
2b	Cd	ethanol	2-methyl	3450 cm^{-1} (v. br., m) 3390 cm^{-1} (br., m) 3315 cm^{-1} (v. br., w) 3227 cm^{-1} (br., vs)	OH – undefined OH – undefined OH \cdots O NH \cdots S
3	Cd	methanol	2-ethyl	3305 cm^{-1} (br., s) 3250 cm^{-1} (br., w) 3189 cm^{-1} (br., vs)	OH \cdots S NH – undefined NH \cdots O
4	Zn	No?	H	3401 cm^{-1} (v. br., vw) 3316 cm^{-1} (v. br., w) 3219 cm^{-1} (br., s)	OH – undefined? OH – undefined? NH \cdots S
5a	Zn	methanol	2-methyl	3298 cm^{-1} (v. br., s) 3248 cm^{-1} (br., w) 3173 cm^{-1} (br., vs)	OH \cdots O NH \cdots S NH \cdots O
5b	Zn	ethanol	2-methyl	3451 cm^{-1} (v. br., m) 3350 cm^{-1} (br., s) 3209 cm^{-1} (v. br., s) 3185 cm^{-1} (br., w)	OH – undefined? OH – undefined? NH \cdots O NH \cdots O
5c	Zn	ethanol	2-methyl	3314 cm^{-1} (br., vs) 3235 cm^{-1} (br., vs)	OH \cdots O NH \cdots S
5d	Zn	2-propa- nol	2-methyl	3364 cm^{-1} (v. br., vs)	OH \cdots S
				3236 cm^{-1} (br., m) 3185 cm^{-1} (br., s)	NH – undefined NH \cdots O
6b	Zn	ethanol	2-ethyl	3397 cm^{-1} (v. br., m) 3359 cm^{-1} (br., w) 3285 cm^{-1} (br., m) 3181 cm^{-1} (br., s)	OH – undefined OH \cdots S NH – undefined NH \cdots O
6c	Zn	2-propa- nol	2-ethyl	3370 cm^{-1} (v. br., vs) 3247 cm^{-1} (br., m) 3189 cm^{-1} (br., s)	OH \cdots S NH – undefined NH \cdots O

with the expected strengths of the interactions (NH \cdots S weaker than NH \cdots O).

According to the Badger–Bauer relationship, the frequency shift is proportional to the enthalpy of hydrogen bonding involving hydroxy compounds.^[17] Comparison of the ν_{OH} frequencies for free alcohol molecules in the gas phase, liquid alcohol and S_2NZn -bound alcohol that forms an O–H \cdots O hydrogen bond is presented in Table 6. It can be concluded that complexation of alcohol to zinc induces rather small changes in the OH \cdots O bond strength (additional $\Delta\nu_{\text{OH}} = 49$ or 46 cm^{-1}), thus it has little influence on the formation of a strong hydrogen bond, which is very likely to precede alcohol deprotonation in the ADH-mediated reaction.^[18]

Table 6. Comparison of ν_{OH} frequency of alcohol hydroxy group in the systems studied.

System	ν_{OH} [cm^{-1}]	$\Delta\nu_{\text{OH}}$ [cm^{-1}]
methanol (free) ^[19a]	3681	
methanol (liquid film) ^[19c]	3347	334
methanol in 5a ^[a]	3298	383(49)
ethanol (free) ^[19b]	3636	
ethanol (liquid film) ^[19c]	≈ 3360	≈ 276
ethanol in 5c ^[a]	3314	322(46)

[a] This work.

NMR Spectra

The ^1H - and ^{13}C NMR solution spectra of the zinc complexes **4**, **5a** and **6a** show that all these derivatives are kinetically stable on the NMR timescale in CDCl_3 , but undergo slow ligand-exchange processes in CD_3OD (see NMR spectroscopic data in the Experimental Section). For example, the ^{13}C NMR spectrum of **4** in CDCl_3 shows three signals in the aromatic region with similar chemical shifts (117, 127.6 and 136.9 ppm) as those in the solid-state NMR spectra of the cadmium complexes (e.g. Figure 15). The ^1H NMR spectrum of the same solution displays three distinct signals at 7.15, 7.47, 8.02 ppm attributable to the protons at the aromatic ring. Both findings indicate that the exchange of protons between the nitrogen atoms of imidazole is stopped or slowed down as a result of complexation to zinc. In contrast, the ^1H NMR spectrum of the same compound in CD_3OD displays only two signals – a sharp singlet at $\delta = 8.30$ ppm and a very broad one at $\delta = 7.34$ ppm – and the corresponding ^{13}C NMR spectrum exhibits, in addition to a sharp resonance at $\delta = 139.0$ ppm, two very broad signals at 128 and 117 ppm, respectively. This indicates a moderately slow exchange process. The ^{13}C - and ^1H NMR solution spectra of the analogous cadmium complex **1** in CD_3OD exhibit only a single broad (^{13}C) or sharp (^1H) signal for the imidazole C4, C5 or H4, H5 atoms, respectively, which is in accord with an increased exchange rate. As a switchover of protons between the two N-donor sites cannot occur as long as the ligand remains coordinated to the metal, the observed dynamics can be regarded as proof for the occurrence of ligand dissociation, and thus of kinetic instability, of the N-donor moieties, and the rate of

this process is apparently higher in the Cd complexes than in the Zn complexes.

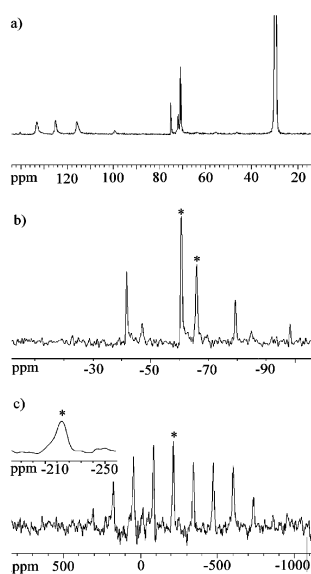


Figure 15. Experimental CP/MAS spectra of **1**: (a) ^{13}C NMR (spinning rate 7 kHz); (b) ^{29}Si NMR (spinning rate 1.5 kHz); (c) ^{113}Cd NMR (spinning rate 13 kHz).

The addition of an increasing amount of imidazole or 2-methylimidazole to $[\text{D}_4]\text{MeOH}$ solutions of **1** and **2a** induced a continuous change in ^{113}Cd chemical shift (Table 7). As in previously published studies,^[7k,9] these results confirm the presence of an equilibrium between a mixture of a (probably dimeric^[9]) cadmium thiolate and imidazole and the corresponding heteroleptic adduct in solution; the formation of the latter occurs with increasing imidazole or 2-methylimidazole concentration.

Table 7. ^{113}Cd NMR shifts for **1**, **2a** and **3** in CD_3OD solution and in the solid state.

	Imidazole derivative	Imidazole concentration [M]	^{113}Cd NMR shift [ppm] ^[a]	^{113}Cd NMR shift [ppm] ^[a]
			Solution	Solid state
1	H	0	395	453
		0.2	433	
		0.4	442	
		0.8	451	
2a	2-methyl	0	405	441, 436, 433, 428
		0,5	429.5	
		1	434	
		2	439	
		4	443	
3	2-ethyl	–	–	428, 418

[a] Relative to 0.1 M $\text{Cd}(\text{ClO}_4)_2$.

The cadmium compounds **1**, **2a** and **3** were also studied by solid-state NMR spectroscopy. The ^{13}C -, ^{29}Si - and ^{113}Cd solid-state NMR spectra of **1**, **2a** and **3** presented in Figures 15a–c, 16a–c and 17a–c are well in accord with the crystal structure. The single crystallographically independent molecule of **1** gives rise to two ^{29}Si NMR signals, and the presence of two crystallographically independent mole-

cules of **2a** and **3** results in the presence of four distinguishable ^{29}Si NMR signals. As expected, the ^{113}Cd NMR spectrum of **1** displays a single resonance, whereas two signals with similar isotropic chemical shifts are observed for **3** (Figures 15c, 17c, Table 8). The individual spinning sidebands in the ^{113}Cd spectra of **2a** display a unique, asymmetric lineshape, which results from a superimposition of at least four overlapping components arising from crystallographically nonequivalent specimen (Figure 16c) with chemical shifts of –225 (441), –230 (436), –233 (433) and –238 (428) ppm [the numbers in parentheses are the ^{113}Cd chemical shifts relative to 0.1 M $\text{Cd}(\text{ClO}_4)_2$]. As deconvolution was unfeasible, the data were processed by applying extensive line broadening prior to FT, in order to collapse the observed line profile into a single averaged spinning sideband manifold. The isotropic and anisotropic chemical shift values that were calculated from these data (listed in Table 8) must thus be considered to represent average values of all crystallographically nonequivalent specimens present. We believe that the observed complication of the spectra arises again from the loss of methanol that has been detected as the first coordination sphere ligand of the cadmium ion during the X-ray diffraction studies. However, whereas the samples used in these experiments had been prepared by quickly transferring crystalline complexes directly from the cold mother liquor into a cold stream of nitrogen, the samples for the solid-state NMR measurements were finely ground at room temperature, and it ap-

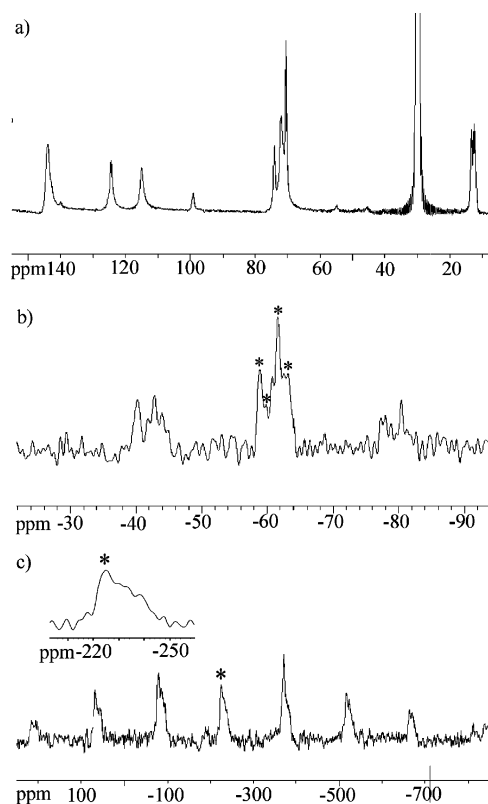


Figure 16. Experimental CP/MAS spectra of **2a**: (a) ^{13}C NMR (spinning rate 7 kHz); (b) ^{29}Si NMR (spinning rate 1.5 kHz); (c) ^{113}Cd NMR (spinning rate 13 kHz).

pears highly likely that loss of the weakly bound methanol ligands occurred during this procedure. This assumption is further in accord with the observation that no signal for the methanol carbon was observed in the solid-state ^{13}C NMR spectra of all three cadmium complexes.

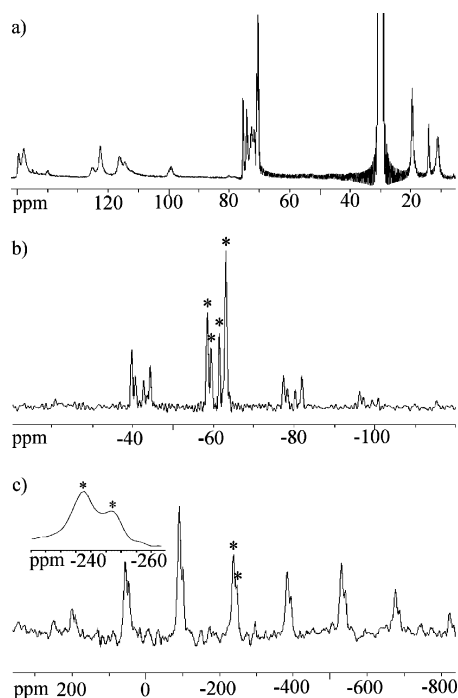


Figure 17. Experimental CP/MAS spectra of **3**: (a) ^{13}C NMR (spinning rate 7 kHz); (b) ^{29}Si NMR (spinning rate 1.5 kHz); (c) ^{113}Cd NMR (spinning rate 13 kHz).

The ^{113}Cd chemical shift value in the solid state is the same as that reached at a maximum concentration of the added N ligand in solution (Table 7). One of the isotropic ^{113}Cd chemical shifts of solid **2a** ($\delta = 441$ ppm) as well as the ^{113}Cd NMR chemical shift of a methanol solution of **2a** ($\delta = 443$, in the presence of a large excess of 2-methylimidazole) are very close to that of the ^{113}Cd -substituted LADH-NAD⁺ complex ($\delta = 442$ ppm).^[2a] The change in the ^{113}Cd chemical shift from 451 ppm in **1** to 418 ppm in **3** follows the order of increasing basicity of the N ligands: imidazole ($\text{p}K_{\text{b}} = 7.01$) < 2-methylimidazole ($\text{p}K_{\text{b}} = 6.15$) < 2-ethylimidazole ($\text{p}K_{\text{b}} = 6.00$); all $\text{p}K_{\text{b}}$ values are from the literature.^[20] The isotropic shifts δ_{iso} , the values of the principal components δ_{ii} and the anisotropy parameters $\Omega = \delta_{11} - \delta_{33}$ and $\kappa = (\delta_{22} - \delta_{\text{iso}})/(\delta_{11} - \delta_{33})$ of the ^{113}Cd shield-

ing tensors are gathered in Table 8. Large Ω values, which are similar for all of the cadmium compounds studied, indicate a low symmetry of the coordination environment of the cadmium ion (see ref.^[7k] for discussion). The complete ^{13}C - and ^{29}Si NMR spectroscopic data for the cadmium complexes are listed in Tables S3 and S4 in the Supporting Information.

HF and DFT Calculations – Enthalpies of Deprotonation as a Relative OH Acidity Measure

Our aim was to examine the extent to which zinc complexation of the alcohol facilitates its stepwise dehydrogenation in the enzyme alcohol dehydrogenase. First the ab initio RHF method was employed with use of effective core potentials of Stevens, Basch, Krauss, Jasien and Cundari (SBKJIC) for all heavy atoms,^[21] together with the SBKJIC basis set as implemented in the GAMESS package.^[22] Subsequently, DFT calculations were performed with the hybrid B3LYP functional, by using the same pseudopotentials and basis set. The alcohol deprotonation enthalpy in vacuo has been calculated as the reference state. The experimental value for this process is known as 1579.5 kJ/mol^[23] and is compared with the calculated deprotonation enthalpies for a molecule of ethanol that is hydrogen bonded to the oxygen atom in S-methylated tri-*tert*-butoxysilanethiol and with the ethanol molecule in complex **5c**, which we consider as an accurate structural model for the ADH active site.

The calculated enthalpies ΔH for the deprotonation of EtOH calculated at the ab initio and DFT levels are: (a) $\Delta H_{\text{a}} = 1649.87$ kJ/mol (HF) and 1612.6 kJ/mol (DFT) for ethanol in vacuo; (b) $\Delta H_{\text{b}} = 1581.47$ kJ/mol (HF) and 1535.8 kJ/mol (DFT) for ethanol hydrogen bonded to S-methylated tri-*tert*-butoxysilanethiol; (c) $\Delta H_{\text{c}} = 1241.2$ kJ/mol (HF) and 1438.66 kJ/mol (DFT) for the ethanol molecule in **5c**.

Deprotonation of the zinc-bound alcohol is probably the first step, preceding hydride transfer, during the alcohol dehydrogenation catalysed by LADH.^[24] The difference between ΔH_{b} and ΔH_{c} represents the contribution of the zinc ion to a decrease in the deprotonation enthalpy of ethanol in our model systems. Quantum mechanical calculations indicate the decrease is by about 20% (340.2 kJ/mol) for HF or by even only 10% (173.94 kJ/mol) for DFT. Thus, the contribution of the zinc ion to the decrease in the overall energy barrier for dehydrogenation does not seem to be very great, and this effect alone cannot explain the effi-

Table 8. Isotropic ^{113}Cd chemical shifts δ_{iso} , values of the principal components δ_{ii} , and anisotropy parameters Ω and κ of the ^{113}Cd magnetic shielding tensors.

	$\delta_{\text{iso}}^{\text{[a]}}$	$\delta_{11}^{\text{[a]}}$	$\delta_{22}^{\text{[a]}}$	$\delta_{33}^{\text{[a]}}$	Ω	κ
1	-213.3 (453)	345 (1011)	-175 (491)	-810 (-144)	1155	0.10
2a ^[b]	-229.3 (438)	288 (954)	-209 (457)	-767 (-101)	1055	0.06
3	-237.5 (428.5)	253 (919)	-126 (540)	-839 (-173)	1118	0.27
	-247.8 (418)	260 (926)	-146 (520)	-858 (-192)	1092	0.31

[a] $\delta^{113}\text{Cd}$ values vs. CdMe_2 ($\mathcal{E} = 22.193175$ MHz); values in parentheses denote chemical shifts vs. 0.1 M $\text{Cd}(\text{ClO}_4)_2$; (see Experimental Section). [b] Averaged over the line profile, which results from superposition of unresolved resonances of different crystallographically nonequivalent specimens.

ciency of LADH. It is certainly a part of the working machinery and other important contributions come from: (i) the closure of LADH domains to separate the active site from bulk water^[1b]; (ii) a proton relay system – the net of hydrogen bonds helps to remove the proton from the alcohol molecule complexed to the zinc ion, and hydrogen bonds within this system are probably much stronger than those present in our model;^[18] (iii) the NAD⁺ docking system, the molecule is properly oriented towards the alcoholate in the active site – there are hydrophilic amino acids, which form hydrogen bonds with NAD⁺, and hydrophobic residues behind the nicotinamide ring, which push the ring towards C1 of the substrate to allow hydride tunneling.^[25]

By taking the degree of complexity of this system into account, it seems rather obvious that “cutting” the zinc–alcohol complex and the first coordination sphere ligands from LADH is not enough to obtain an efficient catalyst.

HF and PM6 Calculations – Comparison of the Stabilities of Zinc, Cadmium and Mercury Complexes with Oxygen, Nitrogen and Sulfur Ligands

The stability constants of heteroleptic zinc and cadmium complexes in solution were not tested experimentally. However, on the basis of a qualitative comparison of the NMR spectra obtained from solutions of **1** and **4**, a higher stability for the zinc complexes should be expected. In order to compare quantitatively the different 12 group metals in this respect, we determined the theoretical enthalpies for metal ion exchange and formation of zinc, cadmium and mercury complexes with model sulfur, nitrogen and oxygen ligands. Quantum mechanical calculations at the ab initio SBKJJC^[21,22] and semiempirical PM6 Hartree–Fock level^[26] were applied. The results (see Supporting Information) indicate almost uniformly, and in accordance with the NMR spectroscopic data, that the zinc complexes should be the most stable species among the 12 group metal complexes.

Conclusions

We have studied a series of zinc and cadmium heteroleptic complexes resembling the active centre of alcohol dehydrogenase. Their solid-state structures, alcohol binding capabilities, FTIR and NMR spectra, and stability in solution have been investigated. The conclusions are: (i) Zinc and cadmium tri-*tert*-butoxysilanethiolates with 2-methylimidazole as a coligand are capable of alcohol binding, and the binding is reversible. Structural parameters obtained for methanol and ethanol coordinated to zinc and cadmium in a coordination environment that strictly resembles the active site of ADH indicate that cadmium ions easily accommodate more than four ligands in the first coordination sphere and tend to form at least pentacoordinate complexes. The geometry of the zinc complexes with a coordinated alcohol is between tetrahedral and trigonal bipyramidal. It is possible that the differences between the coordination of zinc and cadmium in the studied models resemble those between native and cadmium-substituted LADH. (ii)

Comparison of the obtained model complexes with crystal structures of various ADHs suggests that metal ion in the ADH active site is – at least temporarily – pentacoordinate. The geometry of the zinc ion may be approximated as a trigonal bipyramid; the alcohol (water) and the Glu-68 carboxylate oxygen atom occupy apical positions. (iii) It is possible to identify NH[⋯]S, NH[⋯]O, OH[⋯]S and OH[⋯]O stretching modes in the FTIR spectra of the complexes studied. Complexation of methanol or ethanol to the zinc ion influences the strength of hydrogen bonds formed by the alcohol molecule; however, the presence of an appropriate acceptor is more important. (iv) The solid-state ¹¹³Cd NMR shift of the five-coordinate cadmium complex **2a** with a CdNO₂S₂ coordination core is almost identical to that of cadmium-substituted alcohol dehydrogenase in a complex with NAD⁺, which suggests that the distribution of electron density must be very similar in both species. (v) Quantum mechanical calculations indicate a 10–20% decrease in the enthalpy of ethanol deprotonation because of complexation with Zn²⁺. (vi) On the basis of the NMR spectroscopic studies and calculations at the Hartree–Fock level, it is concluded that with this configuration of ligands, the zinc complexes are more stable than the cadmium and mercury complexes.

Experimental Section

X-ray Diffraction Studies: Diffraction data were recorded on a KUMA KM4 diffractometer with graphite-monochromated Mo-*K*_α radiation, equipped with a Sapphire 2 CCD camera (Oxford Diffraction). Numerical absorption corrections were applied. The structure was solved by direct methods and refined with the SHELX97 program package^[27] by using full-matrix least-squares refinement based on *F*². All non-hydrogen atoms were refined anisotropically. Hydrogen atoms were usually refined in geometrically idealised positions with isotropic temperature factors 1.2 or 1.5 times the equivalent isotropic temperature factors *U*_{eq} of their attached atoms. Crystal data, description of the diffraction experiment and details of the structure refinement are presented in Table 9. There are pronounced differences between the displacement parameters determined for an alcohol molecule complexed to the metal or trapped in the crystal lattice by hydrogen bonds. *U*_{ij} parameters for the latter indicate high mobility of the molecule even at low temperatures (120 K). Problems encountered during the refinement procedure of the cadmium complex **2a** can most probably be explained by the partial “escape” of methanol molecules from the voids they occupy. To overcome this problem, we applied the same procedure that had previously been used for analogous manganese tri-*tert*-butoxysilanethiolate complexes^[7] by setting the occupancy factor of methanol to 0.5. This strategy allowed a stable solution to be found, but the picture obtained in this way certainly implies an averaging procedure since the methanol molecules are most probably absent in some of the voids. By comparing the structures of over 15 tri-*tert*-butoxysilanethiolates with those presented here,^[7] we conclude that the static disorder of the crystal structure is the intrinsic feature of complexes with metal-bound alcohol molecules. CCDC-622858, -692140, -692141, -692142, -692143, -692144, -692145, -692146, -692147 and -692148 contain the supplementary crystallographic data for this paper. These data can be obtained free of charge from The Cambridge Crystallographic Data Centre via www.ccdc.cam.ac.uk/data_request/cif.

Table 9. Crystal data and structure refinement for the complexes studied.

	1	2a	3	4	5a
Empirical formula	C ₂₈ H ₆₂ CdN ₂ O ₇ S ₂ Si ₂	C ₁₁₅ H ₂₅₂ Cd ₄ N ₈ O ₂₇ S ₈ Si ₈	C ₃₀ H ₆₆ CdN ₂ O ₇ S ₂ Si ₂	C ₂₇ H ₅₈ N ₂ O ₆ S ₂ Si ₂ Zn	C ₅₈ H ₁₂₈ N ₄ O ₁₄ S ₄ Si ₄ Zn ₂
Formula weight	771.50	3110.05	799.55	692.42	1476.98
Crystal dimensions [mm]		0.34 × 0.23 × 0.19	0.243 × 0.193 × 0.097	0.198 × 0.096 × 0.003	0.264 × 0.178 × 0.038
Crystal system	orthorhombic	monoclinic	monoclinic	monoclinic	monoclinic
Space group	<i>Pna</i> 2 ₁	<i>P</i> 2 ₁ / <i>n</i>	<i>P</i> 2 ₁ / <i>n</i>	<i>P</i> 2 ₁ / <i>c</i>	<i>P</i> 2 ₁ / <i>n</i>
<i>a</i> [Å]	17.5326(7)	18.5319(11)	19.5068(4)	16.2192(4)	18.5515(3)
<i>b</i> [Å]	8.6735(3)	26.8287(8)	24.7335(4)	8.6472(2)	26.4480(5)
<i>c</i> [Å]	26.7413(10)	18.9517(7)	19.6700(3)	29.7324(9)	18.7446(3)
<i>α</i> [°]	90	90	90	90	90
<i>β</i> [°]	90	117.619(5)	115.804(2)	113.470(2)	115.206(2)
<i>γ</i> [°]	90	90	90	90	90
Volume [Å ³]	4066.5(3)	8348.8(7)	8543.9(3)	3825.00(17)	8321.3(2)
$\rho_{\text{calcd.}}$ [Mg/m ³]	1.260	1.237	1.243	1.202	1.179
<i>Z</i>	4	2	8	4	4
2 θ_{max} [°]	50.08	50.1	50.1	52	50.1
Completeness to θ_{max} [%]	99.9	99.6	98.4	99.8	99.8
Radiation (λ [Å])	Mo- <i>Kα</i> (0.71073)	Mo- <i>Kα</i> (0.71073)	Mo- <i>Kα</i> (0.71073)	Mo- <i>Kα</i> (0.71073)	Mo- <i>Kα</i> (0.71073)
Scan mode	Ω	Ω	Ω	Ω	Ω
Temperature [K]	120(2)	120(2)	120(2)	120(2)	120(2)
Reflections collected/unique	24758/7131	14730/11969	14901/12811	7507/5535	14705/12047
Data/restraints/parameters	7131/1/400	14730/0/756	14901/6/896	7507/0/379	14705/0/815
Absorption coefficient [mm ⁻¹]	0.737	0.718	0.704	0.85	0.787
Transmission min/max		0.802/0.901	0.785/0.865	0.807/0.931	0.737/0.936
Absorption correction	analytical	analytical	analytical	analytical	analytical
Final <i>R</i> indices [<i>I</i> > 2 σ (<i>I</i>)]	<i>R</i> ₁ = 0.0425 <i>wR</i> ₂ = 0.1043	<i>R</i> ₁ = 0.0498 <i>wR</i> ₂ = 0.1312	<i>R</i> ₁ = 0.0426 <i>wR</i> ₂ = 0.11	<i>R</i> ₁ = 0.0353 <i>wR</i> ₂ = 0.812	<i>R</i> ₁ = 0.0416 <i>wR</i> ₂ = 0.1107
<i>R</i> indices (all data)	<i>R</i> ₁ = 0.0429 <i>wR</i> ₂ = 0.1045	<i>R</i> ₁ = 0.0667 <i>wR</i> ₂ = 0.1471	<i>R</i> ₁ = 0.0519 <i>wR</i> ₂ = 0.1213	<i>R</i> ₁ = 0.0554 <i>wR</i> ₂ = 0.991	<i>R</i> ₁ = 0.057 <i>wR</i> ₂ = 0.123
Residual electron density [e Å ⁻³]	2.683/−0.633	1.654/−1.501	1.278/−0.859	0.686/−0.61	2.250/−0.701
	5b	5c	5d	6a	6b
Empirical formula	C ₃₀ H ₆₆ N ₂ O ₇ S ₂ -Si ₂ Zn	C ₅₈ H ₁₂₆ N ₄ O ₁₃ S ₄ Si ₄ Zn ₂	C ₃₁ H ₆₈ N ₂ O ₇ S ₂ Si ₂ Zn	C ₃₀ H ₆₆ N ₂ O ₇ S ₂ Si ₂ Zn	C ₃₁ H ₆₈ N ₂ O ₇ S ₂ Si ₂ Zn
Formula weight	752.52	1458.97	766.54	752.52	766.54
Crystal dimensions [mm]	0.19 × 0.14 × 0.1	0.282 × 0.116 × 0.059	0.309 × 0.177 × 0.075	0.25 × 0.13 × 0.02	0.24 × 0.17 × 0.05
Crystal system	monoclinic	triclinic	monoclinic	monoclinic	monoclinic
Space group	<i>P</i> 2 ₁ / <i>c</i>	<i>P</i> 1	<i>P</i> 2 ₁ / <i>c</i>	<i>P</i> 2 ₁ / <i>c</i>	<i>P</i> 2 ₁ / <i>c</i>
<i>a</i> [Å]	9.5688(3)	14.1422(5)	19.7802(4)	9.6726(3)	19.5467(4)
<i>b</i> [Å]	24.3130(7)	16.1544(6)	24.4923(5)	24.5723(8)	24.6223(5)
<i>c</i> [Å]	19.8441(5)	19.6673(6)	19.7996(4)	19.7595(7)	19.9683(4)
<i>α</i> [°]	90	85.811(3)	90	90	90
<i>β</i> [°]	113.946(2)	72.166(3)	115.100(2)	116.573(3)	116.623(2)
<i>γ</i> [°]	90	80.470(3)	90	90	90
Volume [Å ³]	4219.3(2)	4217.0(3)	8686.4(3)	4200.3(3)	8591.5(3)
$\rho_{\text{calcd.}}$ [Mg/m ³]	1.185	1.149	1.172	1.19	1.185
<i>Z</i>	4	2	8	4	8
2 θ_{max} [°]	50.08	50.1	51	50.1	50.1
Completeness to θ_{max}	99.8	95.1	99.8	98.8	99.1
Radiation (λ [Å])	Mo- <i>Kα</i> (0.71073)	Mo- <i>Kα</i> (0.71073)	Mo- <i>Kα</i> (0.71073)	Mo- <i>Kα</i> (0.71073)	Mo- <i>Kα</i> (0.71073)
Scan mode	Ω	Ω	Ω	Ω	Ω
Temperature [K]	120(2)	120(2)	120(2)	120(2)	120(2)
Reflections collected/independent	7461/6609	14220/10312	46673/15382	7365/6194	15085/12741
Data/restraints/parameters	7461/0/429		15382/0/855	7365/0/418	15085/0/853
Absorption coefficient [mm ⁻¹]	0.777	0.775	0.756	0.781	0.764
Transmission min/max	0.795/0.861	–	0.827/0.925	0.809/0.96	0.774/0.843
Absorption correction	analytical	none	analytical	analytical	analytical
Final <i>R</i> indices [<i>I</i> > 2 σ (<i>I</i>)]	<i>R</i> ₁ = 0.0349 <i>wR</i> ₂ = 0.0935	<i>R</i> ₁ = 0.0553 <i>wR</i> ₂ = 0.1367	<i>R</i> ₁ = 0.0358 <i>wR</i> ₂ = 0.0917	<i>R</i> ₁ = 0.0471 <i>wR</i> ₂ = 0.1263	<i>R</i> ₁ = 0.0357 <i>wR</i> ₂ = 0.0884
<i>R</i> indices (all data)	<i>R</i> ₁ = 0.0421 <i>wR</i> ₂ = 0.101	<i>R</i> ₁ = 0.0871 <i>wR</i> ₂ = 0.1572	<i>R</i> ₁ = 0.0480 <i>wR</i> ₂ = 0.0988	<i>R</i> ₁ = 0.0592 <i>wR</i> ₂ = 0.1404	<i>R</i> ₁ = 0.0469 <i>wR</i> ₂ = 0.0972
Residual electron density [e Å ⁻³]	0.702/−0.488	0.966/−1.02	0.724/−0.544	1.444/−0.545	0.672/−0.478

FTIR Studies: The FTIR spectra of crystalline samples were measured with a Momentum microscope connected to a Genesis II spectrometer (Mattson). FTIR ATR spectra of tri-*tert*-butoxysilanethiol/methanol and imidazole/methanol mixtures were recorded on a Nicolet 8700 FTIR spectrometer. The OH and NH stretching regions were analysed by using the commercial programs GRAMS/32 (Galactic Industries Corporation, Salem) and RAZOR (Spectrum Square Associates, Ithaca) run under GRAMS/32. All peaks in the analysed region of the experimental spectra were approximated with the product of Gaussian and Lorentzian peak functions.

Solid-State NMR Studies: Solid-state CP/MAS-NMR spectra were recorded on a Bruker Avance 400 MHz NMR spectrometer with spinning speeds of 1.5 (^{29}Si), 7 (^{13}C) and 11–14 kHz (^{113}Cd). Cross polarisation with a ramp-shaped contact pulse and mixing times between 1.8 and 5 ms was used for signal enhancement. Chemical shifts were referenced to external TMS (^1H , ^{29}Si) or CdMe_2 ($\mathcal{E} = 22.193175$ MHz, ^{113}Cd), respectively; cadmium formate was used as a secondary standard for the ^{113}Cd NMR measurements. The ^{113}Cd chemical shifts were also recalculated with respect to 0.1 M $\text{Cd}(\text{ClO}_4)_2$ as a standard by using the formula:^[28] $\delta[\text{Cd}(\text{ClO}_4)_2] = \delta(^{113}\text{Cd}) + 666$. The position of the isotropic lines in the ^{113}Cd NMR spectra was verified by comparing line positions in spectra recorded with different spinning speeds. Anisotropic ^{113}Cd shift parameters were determined by fitting the intensity profiles of the spinning sideband manifolds by using a simplex fit algorithm provided with the TOPSPIN 1.3 spectrometer software.

Solution NMR Studies: ^1H -, ^{13}C -, ^{29}Si - and ^{113}Cd spectra of the cadmium compounds were obtained at the Institut für Anorganische Chemie, University of Karlsruhe, with a Bruker Av400 spectrometer. ^1H - and ^{13}C spectra of the zinc compounds were measured on a Gemini 200 spectrometer. ^1H -, ^{13}C - and ^{29}Si NMR spectra were referenced to TMS. ^{113}Cd NMR spectra were referenced to external 0.1 M $\text{Cd}(\text{ClO}_4)_2$ in D_2O as a secondary standard, and recalculated by using CdMe_2 ($\mathcal{E} = 22.193175$ MHz, ^{113}Cd) as a reference.

Computational Details: The ab initio Hartree–Fock and DFT SBKJC pseudopotential calculations^[21] were performed with the GAMESS (version 22) package.^[22] The crystallographic structure was used to obtain a starting geometry where possible; otherwise, the final geometry from a previous PM6 calculation was used. Semiempirical Hartree–Fock PM6 calculations were performed with the MOPAC 2007 (version 7.155 w) package.^[26]

Substrates and Solvents: Tri-*tert*-butoxysilanethiol, $(t\text{BuO})_3\text{SiSH}$, was obtained by alcoholysis of SiS_2 .^[29] Zinc acetylacetonate (melting point 126 °C) was prepared from ZnO, and freshly distilled acetylacetonate as described previously.^[30] Cadmium tri-*tert*-butoxysilanethiolate $\text{Cd}_2(\text{RS})_4$: $\text{CdCl}_2 \cdot 2.5\text{H}_2\text{O}$ (0.92 g, 4 mmol) was dissolved in water, and triethylamine (5.8 mL, 42 mmol) and tri-*tert*-butoxysilanethiol (4.24 mL, 14 mmol) were added to the solution. The reaction mixture was vigorously shaken for 5 min. The resulting precipitate of $\text{Cd}_2(\text{RS})_4$ was separated by filtration, dried and recrystallised from hexane. M.p. 208 °C. Yield: 30%. Solvents were purchased from Sigma–Aldrich (GC 99.9% purity grade).

Complexes: The yield of all the syntheses was approximately 20–30%. Each time, the first crop of crystals was collected, and no effort was undertaken to optimise the conditions of the reactions or crystallisation to increase the yields of reactions.

[Cd{SSi(*ORu*)₃}₂(C₃H₄N₂)}·CH₃OH (1): $\text{Cd}_2(\text{RS})_4$ (0.5 mmol) was dissolved in a solution of imidazole (2 mmol) in MeOH (15 mL). The resulting solution was filtered, an equal volume of acetonitrile

was added, and the reaction mixture was stored at –18 °C. After 24 h, colourless plates of **1** formed. M.p. 210–211 °C (dec.). $\text{C}_{28}\text{H}_{62}\text{CdN}_2\text{O}_7\text{S}_2\text{Si}_2$ (771.5): calcd. C 43.59, H 8.10, N 3.63, S 8.31; found C 43.73, H 8.06, N 3.81, S 8.55. IR (single crystal): $\tilde{\nu} = 3178$ (br. m, sh.), 3134 (m, br.), 3061 (m), 3031 (vw), 2978 (vs), 2931 (s), 2906 (s), 2871 (s), 2604 (w), 2273 (w), 1740 (w), 1716 (w), 1699 (w), 1683 (vw), 1671 (w), 1653 (vw), 1620 (w, br.), 1557 (vw), 1541 (m), 1536, 1506 (m), 1473 (s), 1440 (m), 1390 (vs), 1368 (vs), 1361 (vs, sh.), 1331 (m), 1239 (vs), 1187 (vs, br.), 1147 (m), 1099 (m), 1070 (vs, sh.), 1036 (vs, br.), 1025 (vs, sh.), 983 (s), 945 (m, sh.), 915 (m), 866 (w) 839 (m, sh.), 821 (s), 802 (s), 756 (s) cm^{-1} . ^1H NMR (400 MHz, CD_3OD): $\delta = 1.40$ [s, 54 H, $\text{C}(\text{CH}_3)_3$], 4.61 (s, 1 H, NH), 7.25 (s, 2 H, CH), 8.04 (s, 1 H, CH) ppm. ^{13}C NMR (100.6 MHz, CD_3OD): $\delta = 30.66$ (s, C–CH₃, tri-*tert*-butoxysilanethiol), 73.70 (s, C–CH₃, tri-*tert*-butoxysilanethiol), 121.47 (s, N–C–N), 136.39 (s, N–C–N) ppm. Solid-state NMR results are described in the text.

{Cd[(*t*BuO)₃SiS]₂(C₄H₆N₂)}·CH₃OH{Cd[(*t*BuO)₃SiS]₂(C₄H₆N₂)-(CH₃OH)} (2a): $\text{Cd}_2(\text{RS})_4$ (0.5 mmol) was dissolved in a solution of 2-methylimidazole (4 mmol) in MeOH (15 mL). The resulting solution was filtered, an equal volume of acetonitrile was added, and the reaction mixture stored at –30 °C. Colourless plates of **1** formed within 24 h. M.p. 224–225 °C (dec. to CdS). $\text{C}_{58}\text{H}_{128}\text{Cd}_2\text{N}_4\text{O}_{14}\text{S}_4\text{Si}_4$ (1572): calcd. C 44.34, H 8.21, N 3.57, S 8.16; found C 44.65, H 8.10, N 3.69, S 8.31. IR (single crystal): Supporting Information. ^1H NMR (400 MHz, CD_3OD): $\delta = 1.39$ [s, 54 H, $\text{C}(\text{CH}_3)_3$], 2.67 (s, 3 H, C–CH₃), 7.17 (s, 2 H, CH) ppm. $^{13}\text{C}\{^1\text{H}\}$ NMR (100.6 MHz, CD_3OD): $\delta = 12.75$ (s, C–CH₃, 2-methylimidazole), 30.67 (s, C–CH₃, tri-*tert*-butoxysilanethiol), 73.60 (s, C–CH₃, tri-*tert*-butoxysilanethiol), 146.07 (s, N–C–N) ppm. ^1H NMR (200 MHz, C_6D_6): $\delta = 1.56$ [s, 54 H, $\text{C}(\text{CH}_3)_3$], 2.59 (s, 3 H, C–CH₃), 6.18 (s, 1 H, CH) 7.73 (s, 1 H, CH) ppm. $^{13}\text{C}\{^1\text{H}\}$ NMR (50.29 MHz, C_6D_6): $\delta = 14.44$ (s, C–CH₃, 2-methylimidazole), 32.26 (s, C–CH₃, tri-*tert*-butoxysilanethiol), 74.54 (s, C–CH₃, tri-*tert*-butoxysilanethiol), 117.8 (s, N–C–N), 146.75 (s, N–C–N) ppm. ^1H NMR (200 MHz, CDCl_3): $\delta = 1.32$ [s, 54 H, $\text{C}(\text{CH}_3)_3$], 2.74 (s, 3 H, C–CH₃, 2-methylimidazole), 3.48 (s, 3 H, CH₃, methanol) 7.15 (s, 2 H, CH) ppm. $^{13}\text{C}\{^1\text{H}\}$ NMR (50.29 MHz, CDCl_3): $\delta = 14.54$ (s, C–CH₃, 2-methylimidazole), 31.93 (s, C–CH₃, tri-*tert*-butoxysilanethiol), 51.14 (s, CH₃, methanol), 74.47 (s, C–CH₃, tri-*tert*-butoxysilanethiol), 146.92 (s, N–C–N) ppm. Solid-state NMR results are described in the text. IR (solid state): Supporting Information.

{Cd[(*t*BuO)₃SiS]₂(C₄H₆N₂)}·C₂H₅OH (2b): This was prepared as described for **2a** with the use of ethanol instead of methanol. Colourless plates. M.p. 206–208 °C (dec. to CdS). IR (solid state): Supporting Information.

{Cd[(*t*BuO)₃SiS]₂(C₅H₈N₂)}·CH₃OH (3): $\text{Cd}_2(\text{RS})_4$ (0.5 mmol) was dissolved in a solution of 2-ethylimidazole (4 mmol) in MeOH (15 mL). The resulting solution was filtered, an equal volume of acetonitrile was added, and the reaction mixture was stored at –30 °C. After 24 h colourless plates of **1** formed. M.p. 184–191 °C (dec. to CdS). $\text{C}_{30}\text{H}_{66}\text{CdN}_2\text{O}_7\text{S}_2\text{Si}_2$ (799.55): calcd. C 45.06, H 8.32, N 3.50, S 8.02; found C 45.51, H 8.47, N 3.60, S 8.05. IR (single crystal): Supporting Information. ^1H NMR (200 MHz, CD_3OD): $\delta = 1.29$ (t, 3 H, CH₃, 2-ethylimidazole), 1.37 [s, 54 H, $\text{C}(\text{CH}_3)_3$], 3.1 (q, 2 H, CH₂, 2-ethylimidazole) 4.9 (s, 1 H, NH) ppm. $^{13}\text{C}\{^1\text{H}\}$ NMR (50.29 MHz, CD_3OD): $\delta = 13.68$ (s, CH₂–CH₃, 2-ethylimidazole), 22.74 (s, CH₂–CH₃, 2-ethylimidazole), 32.35 (s, C–CH₃, tri-*tert*-butoxysilanethiol), 75.26 (s, C–CH₃, tri-*tert*-butoxysilanethiol), 121.5 (s, N–C–N), 151.5 (s, N–C–N) ppm. Solid-state NMR results are described in the text. IR (solid state): Supporting Information.

Zinc Complexes: The syntheses are described only for the methanol solvates. The ethanol and 2-propanol solvates **5b**, **5c**, **5d**, **6b** and **6c** were prepared with the use of the corresponding alcohol instead of methanol.

{Zn[(*t*BuO)₃SiS]₂(C₅H₈N₂)} (**4**): Zn(acac)₂ (2 mmol) was suspended in warm methanol (15 mL), and tri-*tert*-butoxysilanethiol (6 mmol) was added. The contents of the flask were gently shaken until the solution was clear. Imidazole (2 mmol) in methanol (5 mL) was then added. The solution was filtered, and acetonitrile (5 mL) was added. After the solution was stored at –18 °C, colourless, needle-like crystals of **4** were obtained after approximately 24 h. M.p. 218 °C (dec.). C₂₇H₅₉N₂O₆S₂Si₂Zn (693.50): calcd. C 46.83, H 8.44, N 4.04, S 9.26; found C 46.80, H 8.46, N 4.03, S 9.21. IR (single crystal): Supporting Information. ¹H NMR (200 MHz, CDCl₃): δ = 1.36 [s, 54 H, C(CH₃)₃], 7.15 (s, 1 H, N–CH–CH–NH), 7.47 (s, 1 H, N–CH–CH–NH), 8.02 (s, 1 H, N–CH–NH) ppm. ¹H NMR (200 MHz, CD₃OD): δ = 1.39 [s, 54 H, C(CH₃)₃], 7.34 [s, 2 H, N(CH₂)₂N], 8.30 (s, 1 H, N–CH–NH) ppm. ¹³C{¹H} NMR (50.29 MHz, CDCl₃): δ = 31.88 (s, C–CH₃), 31.94 (s, C–CH₃), 74.93 (s, C–CH₃), 117.04 (s, N–C–C–NH), 127.61 (s, N–C–C–NH), 136.90 (s, N–CH–NH) ppm. ¹³C{¹H} NMR (50.29 MHz, CD₃OD): δ = 32.32 (s, C–CH₃), 75.16 (s, C–CH₃), 117.5 (br. s, N–C–C–NH), 128 (br. s, N–C–C–NH), 139.01 (s, N–CH–NH) ppm. IR (solid state): Supporting Information.

{Zn[(*t*BuO)₃SiS]₂(C₄H₆N₂)}·CH₃OH{Zn[(*t*BuO)₃SiS]₂(C₄H₆N₂)(CH₃OH)} (**5a**): Zn(acac)₂ (2 mmol) was suspended in warm methanol (20 mL), and tri-*tert*-butoxysilanethiol (6 mmol) was added. The contents of the flask were gently shaken until the solution was clear. 2-Methylimidazole (4 mmol) in methanol (5 mL) was then added to the reaction mixture. The solution was filtered, and acetonitrile (5 mL) was added. The solution, placed at –18 °C, yielded colourless, crystalline plates of **5a** after approximately 24 h. M.p. slow decomposition. C₅₈H₁₂₈N₄O₁₄S₄Si₄Zn₂ (1476.98): calcd. C 47.16, H 8.74, N 3.79, S 8.68; found C 47.43, H 8.76, N 3.90, S 8.68. IR (single crystal): Supporting Information. ¹H NMR (200 MHz, CDCl₃): δ = 1.35 [s, 54 H, C(CH₃)₃], 2.83 (s, 3 H, C–CH₃, 2-methylimidazole), 3.51 (d, 3 H, CH₃, methanol), 6.92 (s, 1 H, CH), 7.59 (s, 1 H, CH), 9.97 (s, 1 H, NH?, OH?) ppm. ¹H NMR (200 MHz, CD₃OD): δ = 1.35 [s, 54 H, C(CH₃)₃], 2.76 (s, 3 H, CH₃, 2-methylimidazole), 7.12 [s, 2 H, N(CH₂)₂N] ppm. ¹³C{¹H} NMR (50.29 MHz, CDCl₃): δ = 14.43 (s, C–CH₃, 2-methylimidazole), 31.90 (s, C–CH₃, tri-*tert*-butoxysilanethiol), 51.28 (s, CH₃, methanol), 74.60 (s, C–CH₃, tri-*tert*-butoxysilanethiol), 74.93 (s, C–CH₃, tri-*tert*-butoxysilanethiol), 115.22 (s, N–C–C–N), 128.54 (s, N–C–C–N), 147.04 (s, N–C–N) ppm. ¹³C{¹H} NMR (50.29 MHz, CD₃OD): δ = 14 (s, C–CH₃, 2-methylimidazole), 32.30 (s, C–CH₃, tri-*tert*-butoxysilanethiol), 75.17 (s, C–CH₃, tri-*tert*-butoxysilanethiol), 118 and 124 (v br. and hardly visible s, N–C–C–N), 144 (s, N–CH–NH) ppm. IR (solid state): Supporting Information.

{Zn[(*t*BuO)₃SiS]₂(C₄H₆N₂)}·C₂H₅OH (5b**):** (acetonitrile 50% v/v, temperature of crystallisation –18 °C). M.p. 199–202 °C. C₃₀H₆₆N₂O₇S₂Si₂Zn (752.52): calcd. C 47.88, H 8.84, N 3.72, S 8.52; found C 47.76, H 8.81, N 3.73, S 8.47. IR (solid state): Supporting Information.

{Zn[(*t*BuO)₃SiS]₂(C₄H₆N₂)}{Zn[(*t*BuO)₃SiS]₂(C₄H₆N₂)(C₂H₅OH)} (**5c**): (acetonitrile 20% v/v, temperature of crystallisation –30 °C). M.p. 199–202 °C. C₅₈H₁₂₈N₄O₁₃S₄Si₄Zn₂ (1459.04): calcd. C 47.75, H 8.70, N 3.84, S 8.79; found C 46.47, H 8.68, N 3.87, S 8.81. IR (solid state): Supporting Information.

{Zn[(*t*BuO)₃SiS]₂(C₄H₆N₂)}·C₃H₇OH (5d**):** Slow decomposition above 200 °C. M.p. 234–235 °C. C₃₁H₆₈N₂O₇S₂Si₂Zn (766.54):

calcd. C 48.57, H 8.94, N 3.65, S 8.37; found C 48.10, H 8.80, N 3.79, S 8.64. IR (solid state): Supporting Information.

{Zn[(*t*BuO)₃SiS]₂(C₅H₈N₂)}·CH₃OH (6a**):** Zn(acac)₂ (2 mmol) was suspended in warm methanol (10 mL), and tri-*tert*-butoxysilanethiol (6 mmol) was added. The contents of the flask were gently shaken until the solution was clear. 2-Ethylimidazole (4 mmol) in methanol (5 mL) was then added to the reaction mixture. The solution was filtered and acetonitrile (5 mL) was added. The solution, placed at –18 °C, yielded colourless, crystalline plates of **6a** after approximately 24 h. M.p. 200–203 °C. C₃₀H₆₆N₂O₇S₂Si₂Zn (752.52): calcd. C 47.88, H 8.84, N 3.72, S 8.52; found C 48.00, H 8.90, N 3.86, S 8.49. IR (single crystal): Supporting Information. ¹H NMR (200 MHz, CDCl₃): δ = 1.32 [s, 54 H, C(CH₃)₃], 1.35 (triplet-like, 3 H, CH₃, 2-ethylimidazole), 3.28 (q, 2 H, CH₂, 2-ethylimidazole), 3.49 (s, 3 H, CH₃, methanol), 4.38 (s, 1 H, OH), 6.94 (s, 1 H, NCHCHN), 7.54 (s, 1 H, NCHCHN), 10.08 (s, 1 H, NH) ppm. ¹H NMR (200 MHz, CD₃OD): δ = 1.34 [s, 54 H, C(CH₃)₃], 1.39 (s, 3 H, CH₃, 2-ethylimidazole), 3.26 (q, 2 H, CH₂, 2-ethylimidazole), 4.90 (s, 3 H, CH₃, methanol), 7.07 (s, 1 H, NCHCHN), 7.50 (s, 1 H, NCHCHN) ppm. ¹³C{¹H} NMR (50.29 MHz, CDCl₃): δ = 12.95 (s, CH₂–CH₃, 2-ethylimidazole), 21.38 (s, CH₂–CH₃, 2-ethylimidazole), 31.92 (s, C–CH₃, tri-*tert*-butoxysilanethiol), 51.23 (s, CH₃, methanol), 74.46 (s, C–CH₃, tri-*tert*-butoxysilanethiol), 74.93 (s, C–CH₃, tri-*tert*-butoxysilanethiol), 115.32 (s, N–C–C–N), 128.27 (s, N–C–C–N), 151.92 (s, N–C–N) ppm. ¹³C{¹H} NMR (50.29 MHz, CD₃OD): δ = 13.30 (s, CH₂–CH₃, 2-ethylimidazole), 22.49 (s, CH₂–CH₃, 2-ethylimidazole), 32.35 (s, C–CH₃, tri-*tert*-butoxysilanethiol), 75.13 (s, C–CH₃, tri-*tert*-butoxysilanethiol), 116 (s, N–C–C–N), 129 (s, N–C–C–N), 153.22 (s, N–C–N) ppm. IR (solid state): Supporting Information.

{Zn[(*t*BuO)₃SiS]₂(C₅H₈N₂)}·C₂H₅OH (6b**):** M.p. 199–202 °C. C₃₁H₆₈N₂O₇S₂Si₂Zn (766.54): calcd. C 48.57, H 8.94, N 3.65, S 8.37; found C 48.58, H 8.95, N 3.65, S 8.32. IR (single crystal): Supporting Information. ¹H NMR (200 MHz, CDCl₃): δ = 1.25 (t, 6 H, CH₃ ethanol and 2-ethylimidazole), 1.34 [s, 41 H, C(CH₃)₃], 1.35 [s, 13 H, C(CH₃)₃], 3.32 (q, 2 H, CH₂, 2-ethylimidazole), 3.75 (sex., 2 H, CH₂, ethanol), 6.94 (s, 1 H, NCHCHN), 7.59 (s, 1 H, NCHCHN), 9.54 (s, 1 H, NH) ppm. ¹³C{¹H} NMR (50.29 MHz, CDCl₃): δ = 12.73 (s, CH₂–CH₃, 2-ethylimidazole), 18.83 (s, CH₂–CH₃, ethanol), 21.38 (s, CH₂–CH₃, 2-ethylimidazole), 31.92 (s, C–CH₃, tri-*tert*-butoxysilanethiol), 59.1 (s, CH₂, ethanol), 74.59 (s, C–CH₃, tri-*tert*-butoxysilanethiol), 74.92 (s, C–CH₃, tri-*tert*-butoxysilanethiol), 115.01 (s, N–C–C–N), 128.77 (s, N–C–C–N), 152.05 (s, N–C–N) ppm. IR (solid state): Supporting Information.

{Zn[(*t*BuO)₃SiS]₂(C₅H₈N₂)}·C₃H₇OH (6c**):** M.p. 199–200 °C. C₃₂H₇₀N₂O₇S₂Si₂Zn (780.60): calcd. C 48.57, H 8.94, N 3.65, S 8.37; found C 48.58, H 8.95, N 3.65, S 8.32. IR (solid state): Supporting Information.

Supporting Information (see footnote on the first page of this article): Additional experimental details such as structures, FTIR spectra for all compounds, ¹³C- and ²⁹Si solid-state NMR shifts and HF and PM6 calculation results are present.

Acknowledgments

A. D. is very grateful to Dr. Eberhard Matern and Ms. Helga Berberich from the Institut für Anorganische Chemie, University of Karlsruhe (TH), Karlsruhe for the NMR measurements. A. D. also thanks Professor Jerzy Piekies for continuous help. Financial support from the Polish Ministry of Science and Higher Education Grant No. N N204 274835 is acknowledged.

- [1] a) I. Bertini, C. Luchinat, "The Reaction Pathways of Zinc Enzymes and Related Biological Catalysts" in *Bioinorganic Chemistry* (Eds.: I. Bertini, H. B. Gray, S. J. Lippard, J.S. Valentine), University Science Books, Mill Valley, CA, USA, **1994**, pp. 37–106; b) G. Pettersson, *CRC Crit. Rev. Biochem.* **1987**, *21*, 349–389 and papers cited therein; c) R. Meijers, E. S. Cedergren-Zeppezauer, "Zn-Dependent Medium-Chain Dehydrogenases/Reductases" in *Handbook of Metalloproteins* (Eds.: A. Messerschmidt, W. Bode, M. Cygler), **2004**, pp. 5–33, John Wiley & Sons, Ltd., Chichester, U. K.; d) D. S. Auld, T. Bergman, *Cell. Mol. Life Sci.* **2008**, *65*, 3961–3970.
- [2] a) B. R. Bobsein, R. J. Myers, *J. Biol. Chem.* **1981**, *256*, 5313–5316 and the papers cited therein; b) M. W. Makinen, W. Maret, M. B. Yim, *Proc. Natl. Acad. Sci. USA* **1983**, *80*, 2584–2588; c) W. Maret, *Biochemistry* **1989**, *28*, 9944–9949; d) R. Meijers, R. J. Morris, H. W. Adolph, A. Merli, V. S. Lamzin, E. S. Cedergren-Zeppezauer, *J. Biol. Chem.* **2001**, *276*, 9316–9321; e) R. Meijers, H. W. Adolph, Z. Dauter, K. S. Wilson, V. S. Lamzin, E. S. Cedergren-Zeppezauer, *Biochemistry* **2007**, *46*, 5446–5454.
- [3] H. M. Berman, K. Henrick, H. Nakamura, *Nat. Struct. Biol.* **2003**, *10*, 980; www.pdb.org.
- [4] a) P. L. Coleman, H. Weiner, *Biochemistry* **1973**, *12*, 3466–3472; b) A. J. Sytkowski, B. L. Vallee, *Biochemistry* **1979**, *18*, 4095–4099; c) I. Anderson, W. Maret, M. Zeppezauer, R. D. Brown, S. H. Koenig, *Biochemistry* **1981**, *20*, 3424–3432; d) B. R. Bobsein, R. J. Myers, *J. Biol. Chem.* **1981**, *256*, 5313–5316; e) M. F. Dunn, H. Dietrich, A. K. H. MacGibbon, S. C. Koerber, M. Zeppezauer, *Biochemistry* **1982**, *21*, 354–363; f) W. Maret, *Biochemistry* **1989**, *28*, 9944–9949.
- [5] a) U. Ryde, L. Olsen, K. Nilsson, *J. Comput. Chem.* **2002**, *23*, 1058–1070; b) K. Nilsson, U. Ryde, *J. Inorg. Biochem.* **2004**, *98*, 1539–1546.
- [6] G. Parkin, *Chem. Rev.* **2004**, *104*, 699–767.
- [7] a) B. Becker, K. Radacki, W. Wojnowski, *J. Organomet. Chem.* **1996**, *521*, 39–49; b) B. Becker, A. Zaleska, A. Konitz, W. Wojnowski, *Polyhedron* **2001**, *20*, 2567–2576; c) B. Becker, A. Dołęga, A. Konitz, L. Swinder, W. Wojnowski, *Z. Anorg. Allg. Chem.* **2001**, *627*, 280–286; d) B. Becker, A. Pladzyk, A. Konitz, W. Wojnowski, *Appl. Organomet. Chem.* **2002**, *16*, 517–524; e) A. Dołęga, B. Becker, J. Chojnacki, A. Konitz, W. Wojnowski, *Inorg. Chim. Acta* **2004**, *357*, 461–467; f) A. Dołęga, A. Ciborska, J. Chojnacki, M. Walewski, W. Wojnowski, *Thermochim. Acta* **2005**, *429*, 103–109; g) A. Dołęga, E. Baum, A. Konitz, W. Wojnowski, *Acta Crystallogr., Sect. E* **2005**, *61*, m2582–m2584; h) A. Dołęga, J. Chojnacki, A. Konitz, W. Komuda, W. Wojnowski, *Acta Crystallogr., Sect. E* **2006**, *62*, m636–m639; i) A. Kropidłowska, J. Chojnacki, B. Becker, *Inorg. Chem. Commun.* **2006**, *9*, 383–387; j) A. Kropidłowska, J. Chojnacki, B. Becker, *J. Inorg. Biochem.* **2007**, *101*, 578–584; k) A. Dołęga, K. Baranowska, J. Gajda, S. Kaźmierski, M. Potrzebowski, *Inorg. Chim. Acta* **2007**, *360*, 2973–2982; l) A. Dołęga, M. Wiczerzak, K. Baranowska, *Acta Crystallogr., Sect. E* **2007**, *63*, m1774; m) A. Dołęga, A. Pladzyk, K. Baranowska, M. Wiczerzak, *Inorg. Chem. Commun.* **2008**, *11*, 847–850; n) A. Dołęga, A. Pladzyk, K. Baranowska, K. Majcher, *Acta Crystallogr., Sect. C* **2008**, *64*, m259–m263.
- [8] a) I. G. Dance, *Polyhedron* **1986**, *5*, 1037–1104; b) B. Krebs, G. Henkel, *Angew. Chem. Int. Ed. Engl.* **1991**, *30*, 769–788.
- [9] A. Dołęga, M. Walewski, *Magn. Reson. Chem.* **2007**, *45*, 410–415.
- [10] a) J. Seebacher, M. Shu, H. Vahrenkamp, *Chem. Commun.* **2001**, 1026–1027; b) M. Shu, R. Walz, B. Wu, J. Seebacher, H. Vahrenkamp, *Eur. J. Inorg. Chem.* **2003**, 2502–2511.
- [11] a) L. M. Berreau, M. M. Makowska-Grzyska, A. M. Arif, *Inorg. Chem.* **2001**, *40*, 2212–2213; b) M. M. Makowska-Grzyska, P. C. Jeppson, R. A. Allred, A. M. Arif, L. M. Berreau, *Inorg. Chem.* **2002**, *41*, 4872–4887.
- [12] a) A. J. Ganzhorn, B. V. Plapp, *J. Biol. Chem.* **1988**, *263*, 5446–5454; b) U. Ryde, *Protein Sci.* **1995**, *4*, 1124–1132.
- [13] P. C. Sanghani, H. Robinson, W. F. Bosron, T. D. Hurley, *Biochemistry* **2002**, *41*, 10778–10786.
- [14] M. J. Banfield, M. E. Salvucci, E. N. Baker, C. A. Smith, *J. Mol. Biol.* **2001**, *306*, 239–250.
- [15] J. E. Guy, M. N. Isupov, J. A. Littlechild, *J. Mol. Biol.* **2003**, *331*, 1041–1051.
- [16] References for the PDB entries (www.rcsb.org/pdb/): a) 1HET: see ref.^[2c]; b) HLD: S. Ramaswamy, H. Eklund, B. V. Plapp, *Biochemistry* **1994**, *33*, 5230–5237; c) MG0: J. K. Rubach, B. V. Plapp, *Biochemistry* **2002**, *41*, 15770–15779; d) 2OHX: s. Al-Karadaghi, E. S. Cedergren-Zeppezauer, S. Hovmoller, *Acta Crystallogr., Sect. D* **1994**, *50*, 793; e) 1P1R: T. H. Venkataramaiah, B. V. Plapp, *J. Biol. Chem.* **2003**, *278*, 36699–36706; f) 1YE3: B. V. Plapp, B. R. Savarimuthu, S. Ramaswamy, to be published; g) 2JHF: see ref.^[2c]; h) 1HF3: see ref.^[2c]; i) 1HEU: see ref.^[2c]
- [17] a) R. West, R. H. Baney, *J. Am. Chem. Soc.* **1959**, *81*, 6145–6148; b) R. M. Badger, S. H. Bauer, *J. Chem. Phys.* **1937**, *5*, 839–855.
- [18] W. W. Cleland, P. A. Frey, J. A. Gerlt, *J. Biol. Chem.* **1998**, *273*, 25529–25532.
- [19] a) T. Shimanouchi, *Tables of Molecular Vibrational Frequencies*, National Bureau of Standards Reference Data Series, Vol. I, NBS, Washington DC, **1972**; b) R. Laenen, C. Rauscher, *Chem. Phys. Lett.* **1997**, *274*, 63–70; c) Integrated Spectral Data Base System for Organic Compounds: <http://riodb01.ibase.aist.go.jp/sdbs/cgi-bin/>.
- [20] D. D. Perrin, *Dissociation Constants of Organic Bases in Aqueous Solutions*, Butterworths, London, IUPAC suppl., **1965**.
- [21] a) W. J. Stevens, H. Basch, M. Krauss, *J. Chem. Phys.* **1984**, *81*, 6026–6033; b) W. J. Stevens, H. Basch, M. Krauss, P. Jasien, *Can. J. Chem.* **1992**, *70*, 612–630; c) T. R. Cundari, W. J. Stevens, *J. Chem. Phys.* **1993**, *98*, 5555–5565.
- [22] a) M. W. Schmidt, K. K. Baldridge, J. A. Boatz, S. T. Elbert, M. S. Gordon, J. H. Jensen, S. Koseki, N. Matsunaga, K. A. Nguyen, S. Su, T. L. Windus, M. Dupuis, J. A. Montgomery, *J. Comput. Chem.* **1993**, 1347–1363; b) MS Gordon, M. W. Schmidt, "Advances in Electronic Structure Theory: GAMESS a Decade Later" in *Theory and Applications of Computational Chemistry* (Eds.: G. E. Dykstra, G. Frenking, K. S. Kim, G. E. Scuseria), Elsevier, Amsterdam, **2005** and references cited therein; c) A. A. Granovsky, *PC GAMESS version 7.1*, <http://classic.chem.msu.su/gran/gamess/index.html>.
- [23] J. E. Bartmess, R. T. McIver Jr, *J. Am. Chem. Soc.* **1977**, *99*, 4163–4165.
- [24] a) J. Schmidt, J. Chen, M. DeTraglia, D. Minkel, J. T. McFarland, *J. Am. Chem. Soc.* **1979**, *101*, 3634–3640; b) J. Kvassman, J. G. Pettersson, *Eur. J. Biochem.* **1980**, *103*, 557–564; c) J. Kvassman, G. Pettersson, *Eur. J. Biochem.* **1980**, *103*, 565–575; d) P. K. Agarwal, S. P. Webb, S. Hammes-Schiffer, *J. Am. Chem. Soc.* **2000**, *122*, 4803–4812.
- [25] Z. D. Nagel, J. P. Klinman, *Chem. Rev.* **2006**, *106*, 3095–3118.
- [26] J. J. P. Stewart, *J. Mol. Model.* **2007**, *13*, 1173–1213.
- [27] a) G. M. Sheldrick, *Acta Crystallogr., Sect. A* **1990**, *46*, 467; b) G. M. Sheldrick, *SHELXL-97, Program for the Solution and the Refinement of Crystal Structures from Diffraction Data*, University of Göttingen, Göttingen, **1997**.
- [28] M. F. Summers, *Coord. Chem. Rev.* **1988**, *86*, 46–134.
- [29] R. Piękoś, W. Wojnowski, *Z. Anorg. Allg. Chem.* **1962**, *318*, 212.
- [30] M. Hassanein, I. F. Hewaidy, *Z. Anorg. Allg. Chem.* **1970**, *373*, 80–82.

Received: January 29, 2009
Published Online: July 17, 2009